Selective alcohols production through CO_2 photoreduction using Co_3O_4/TiO_2 photocatalyst exploiting synergetic interactions between Ti^{3+}, Co^{2+} and Co^{3+}

Daniel Montalvo [a], Grisel Corro [a,*], Fortino Bañuelos [a], Octavio Olivares-Xometl [b], Paulina Arellanes [b], Umapada Pal [c]

[a] Instituto de Ciencias, Benemérita Universidad Autónoma de Puebla, 4 sur 104, 72000 Puebla, México
[b] Facultad de Ingeniería Química, Benemérita Universidad Autónoma de Puebla, 4 sur 104, 72000 Puebla, México
[c] Instituto de Física, Benemérita Universidad Autónoma de Puebla, Apdo. Postal J-48, 72570 Puebla, México

A R T I C L E   I N F O

A B S T R A C T

In general, CO_2 photoreduction to produce alcohols has shown low conversion efficiency and low selectivity of the products. In this investigation, Co_3O_4/TiO_2 photocatalysts were used for efficient alcohols production during CO_2 photoreduction with H_2O, using UV or visible light. Photocatalysts characterization by XPS, HTEM, and UV–vis spectroscopy suggested that the high activity of the photocatalysts for ethanol, propanol and iso-propanol production can be attributed to the presence of Ti^{3+}, Co^{2+} and Co^{3+} which, decrease the TiO_2 band-gap energy and the photogenerated electron-hole recombination probability. Ti^{3+}, Co^{2+} and Co^{3+} improve adsorption of CO_2 and of generated CO, on the photocatalyst surface, increasing the formyl-radical formation rate, which is the essential step for alcohols production. The effect of CO_2 photoreduction factors, on alcohol production was evaluated, considering different cobalt concentrations and irradiance intensities, through a design experiment. Results revealed that cobalt concentration and irradiation intensity have a significant effect for the reaction.

1. Introduction

The constant increase of greenhouse gases (GHG) levels in the atmosphere is the main cause of the increasing global warming. Carbon dioxide (CO_2) is the most contributing gas to the GHG effect. Its concentration is about 76% of the total GHG [1]. The GHG constant increase levels results from increasing energy consumption in the world. Nearly 80% of the total energy demand is supplied by burning fossil fuels such as natural-gas, coal, and oil [2]. Fossil fuel burning produces about 87% of total CO_2 emissions [3]. Consequently, atmospheric CO_2 concentration, increased from 280 ppm in the pre-industrial period (1850–1900) to 403 ppm in January 2016, reaching 415 ppm by November 2021 [4]. Moreover, it is estimated that it could reach 750 ppm by the end of the 21st century [5], increasing the global temperature between 4.8 and 8 °C [3,6] due to CO_2 infrared sun-light absorption [7].

The continuous increase in CO_2 concentration in the atmosphere, and the growth in fuel consumption have driven a series of investigations around the world, to find a renewable, clean, abundant, and safe source of fuel, that would result in the reduction of CO_2 global concentration and in the global warming mitigation.

A viable solution for these problems may be the photocatalytic reduction of CO_2 with water (H_2O), through a process called "artificial photosynthesis". Named like this, because it tries to mimic the natural photosynthesis process carried out by plants [8], as it uses the same reagents as natural photosynthesis: CO_2, H_2O, and light. However, in this process, the final products are not carbohydrates, but rather high-energy chemical substances such as hydrogen, hydrogen peroxide, formaldehyde, formic acid, methane, methanol, and, ethanol [9–12], among other light compounds. [13,14].

Among the different photocatalysts used for the photocatalytic reduction of CO_2, titanium dioxide (TiO_2) has been widely studied, mainly due to its wide availability, high chemical stability, high redox potential, corrosion resistance, low cost, and non-toxicity [15,16]. However, the photocatalytic activity of TiO_2 for CO_2 reduction is low, due to it fast rate of electronic recombination, low quantum efficiency, and forbidden band energy of 3.2 eV [17,18], which corresponds to UV radiation with a wavelength lower than 387 nm [8]. Although with limitations, this forbidden band feature allows sunlight to be used as a

* Corresponding author.
E-mail address: griselda.corro@correo.buap.mx (G. Corro).

Table 1
Comparison of chemical properties of gasoline and alcohols [2,32–35].

Properties	Gasoline	Ethanol	Isopropanol	propanol
Molecular formula	C_4-C_{12}	C_2H_5OH	i-C_3H_7OH	C_3H_7OH
Molar mass (g/mol)	95–120	46	60	60
Density (kg/m^3)	710–770	789.4	809.0	809.7
Oxygen content (%)	0	34.8	26.6	26.6
Lower heating (MJ/kg)	43.5	26.77	30.44	30.63
Latent heating (MJ/kg)	0.33	0.904	-	0.727
Boiling point (°C)	40–200	78.5	82	82.3
Octane number	80–99	108	107	97
Cetane number	-	8	-	12–21

radiation source to activate TiO_2 since wavelengths in this range represent approximately 3–5% of the solar spectrum reaching the surface of the earth [8,15,18,19].

One way to exploit the solar visible light is using transition metals such as Cu [20], Fe [21] Pt, Ru [22], Ag [23], Au [24] to modify semiconductor crystal structures, lending to a displacement of energy band separation towards the visible light region, resulting in a decrease of electron-hole recombination rate and an increase of CO_2 reduction rate.

Within the group of transition metals, used to modify TiO_2 crystal structure, noble metals such as Pt, Pd, Au, and Ag, have been studied as co-catalysts to help charge transfer, due to their specific work function values and low overpotential. However, the high cost of these metals, has limited their use as co-catalysts. Therefore, non-precious metals, such as Fe, Ni, Cu, and Co have been used to promote the photocatalytic reduction of CO_2. [25–27].

Co is one of the cheapest metals (30.16 USD/g with a purity of 99.99%) used to prepare photocatalysts [28]. Wang et al. [29] mention that cobalt-based photocatalytic materials (alloys, oxides, hydroxides, phosphides, sulfides, and molecular complexes) are highly stable and have demonstrated superior co-catalytic performance by increasing the photocatalytic activity of the host semiconductors through the improvement of their conductivity, narrowing their band gap and presenting abundant active sites.

Selective production of alcohols from the CO_2 photoreduction process represents an economically, sustainable alternative to use this gas, as it is possible to obtain a high-energy fuel with a high-octane number such as ethanol, isopropanol, and propanol. In Table 1, the chemical properties of gasoline and alcohols are reported. In this table, it can be seen that alcohols present an octane number similar to, or slightly higher as that of gasoline. Therefore, these alcohols can be used as a gasoline additive. However, CO_2 photoreduction to produce alcohols is still questioned by the low conversion efficiency and the low selectivity of the products [30], which depend mainly on the type and concentration of the photocatalyst, as well as the performance of the reaction that involves the charges separation and charges transfer routes [9,31].

In this study, we investigated the possibility of improving CO_2 photoreduction with H_2O for increasing alcohols production. It is assumed that CO_2 adsorption on the photocatalyst surface is essential in the photocatalytic reduction process, and therefore, the increase in photocatalytic active adsorption sites may increase substantially the subsequent reaction steps of CO_2 photoreduction with H_2O. As CO_2 can coordinate and bind to cobalt sites [36], we investigated the activity of cobalt deposited on TiO_2 photocatalysts for the CO_2 photoreduction with H_2O. The photocatalytic process was studied using different Co concentrations and different photonic radiation sources. Alcohols production was determined analyzing the reaction products using FTIR gas-spectroscopy.

2. Experimental

2.1. Photocatalysts preparation

The Co/TiO_2 photocatalysts were synthesized by TiO_2 incipient impregnation method, using the appropriate amount of $Co(NO_3)_2 \bullet 6 H_2O$ (Merck, 99.9%) solution to obtain nominal 1%Co/TiO_2 and 10% Co/TiO_2. The resulting mixture was stirred magnetically for 30 min at room temperature, after which the mixture was dried at 90 °C overnight. After the drying process, the catalyst was calcined at 900 °C for 4 h in air-flow (100 ml/min). The calcined samples were stocked in dry conditions and labeled as 1%Co_3O_4/TiO_2 and 10% Co_3O_4/TiO_2. A TiO_2 sample, without Co salt solution impregnation was prepared in the same conditions to be used as reference.

2.2. Photocatalysts characterization

2.2.1. High-resolution transmission electron microscopy (HR-TEM)

The high-resolution transmission electron microscopic images of 1% Co_3O_4/TiO_2 and 10% Co_3O_4/TiO_2 were obtained in a JEM-ARM200CF, JEOL microscope (lattice resolution 78 pm, acceleration voltage 200 kV). Before the microscopic analysis, the photocatalysts samples were dispersed in ethanol and drop casting on carbon coated copper grids.

The size distribution histogram of cobalt nanoparticles was estimated by measuring the size of 100 Co particles for each photocatalyst sample. The mean size of cobalt nanoparticles d_{Co} was calculated from Eq. (1):

$$d_{Co} = \frac{\sum V_i}{\sum S_i}\ (nm) \tag{1}$$

where V_i and S_i are the volume and surface area of the ith particle, respectively.

The number of surface Co atoms per gram of photocatalyst was calculated considering the Co dispersion value D_{Co} defined in Eq. (2):

$$D_{Co} = \frac{\text{Number of surface Co } atoms}{\text{Number of Co } atoms} \tag{2}$$

The number of surface Co atoms was estimated, assuming that the cobalt dispersion values D_{Co} can be calculated from the cobalt surface area and the mean Co particle size data d_{Co} (calculated from Eq. 1), according to Eq. 3 [37,38].

$$D_{Co} = \frac{6 \bullet V_{Co}}{a_{Co}} \bullet \frac{1}{d_{Co}} \tag{3}$$

where V_{Co} is the cobalt atomic volume, and a_{Co} is the average surface area occupied by one Co atom. The values of V_{Co} and a_{Co} were calculated as:

$$V_{Co} = M_{Co} \bullet \frac{10^{21}}{\rho \cdot N_A}\ (nm^3) \tag{4}$$

$$a_{Co} = \pi r^2 (nm^2) \tag{5}$$

where M_{Co} is cobalt molecular mass (58.93 g·mol^{-1}), ρ is the cobalt density (8.90 g·cm^{-3}), N_A is de Avogadro's number (6.022×10^{23} mol^{-1}), r is cobalt atomic ratio (0.152 nm).

Using Eqs. (2) and (3), the number of surface Co atoms was estimated.

2.2.2. X-ray photoelectron spectroscopy (XPS)

The X-ray photoelectron spectra (XPS) of the photocatalysts were obtained using an Escalab 200 R electron spectrometer equipped with a hemispherical analyzer, operating in a constant pass energy mode. Monochromatic Mg Kα emission (hv = 1253.6 eV) from the X-ray tube operating at 10 mA and 12 kV was utilized for recording XPS spectra of the samples. To get good signal-to noise ratios, different energy regions
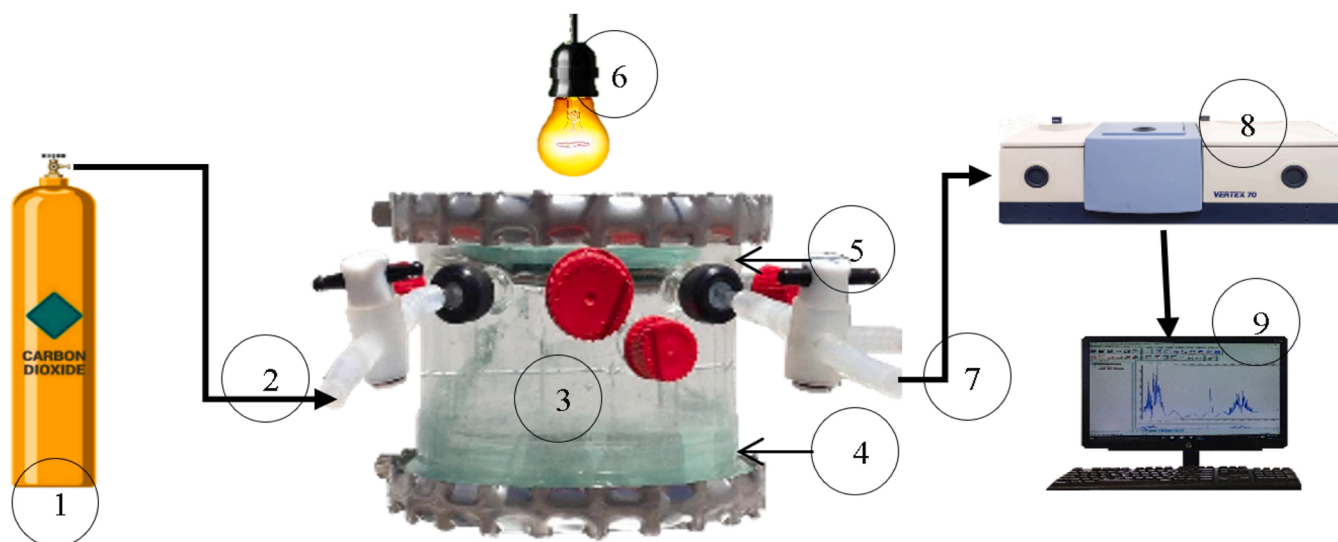
Fig. 1. Experimental setup for photoreduction of CO_2 with H_2O. 1) CO_2 working tank, 2) CO_2 feed flow, 3) Pyrex-glass reactor, 4) Photocatalyst and H_2O 5) Quartz window, 6) Photonic radiation source, 7) Reaction gas outlet, 8) FTIR spectrophotometer, 9) Quantitative determinations.

of the photoelectrons were scanned a number of times.

2.2.3. Photoluminescence spectroscopy

Room temperature photoluminescence spectra of the annealed catalysts were recorded in a FLS 1000 spectrofluorometer of Edinburgh Instruments, with 325 nm excitation from a Xenon-lamp.

2.2.4. Diffuse reflectance spectroscopy UV-Vis (DRIFTS)

Diffuse reflectance spectra were determined on dry-pressed disks (about 15 mm diameter) using a Shimadzu UV-2450 spectrophotometer, equipped with an integrating sphere. Blanks were run with a baseline correction, using $BaSO_4$ as the reference standard. Spectra were obtained at room temperature in a wavelength range of 190–900 nm.

2.3. Photocatalysts band-gap energy estimation

Band-gap energy (E_g) indicates the energy difference between the top of the valence band and the bottom of the conduction band, i.e., it describes the energy necessary to move an electron from the lower energy band (valence band) to a higher energy band (conduction band). Accordingly, band-gap energy value measures the photophysical and photochemical properties of the photocatalysts.

The band-gap energy of the photocatalysts (E_g) was determined by intercepting a fitted straight line in the linear region of the UV–vis spectrum of the sample with the wavelength axis. This intercept value was used to calculate E_g from Planck's equation (Eq. 6).

$$E_g = \frac{hc}{\lambda} = \frac{1239.84 (eV \bullet nm)}{\lambda (nm)} \tag{6}$$

where h is the Planck constant (4.135667×10^{-15} eV•s), c is the light velocity constant in vacuum (2.997924×10^{17} nm•s^{-1}), and λ is the wavelength measured at the interception.

The Tauc method was used to calculate E_g value and the type of transitions of the photocatalysts. In this method, it is established that the absorption coefficient α is energy dependent and can be expressed by Eq. 7 [39].

$$(\alpha h \upsilon)^n = A^* (h \upsilon - E_g) \tag{7}$$

α is defined by the Beer-Lambert's law as $\alpha(\lambda) = (2.303 \cdot A)/\zeta$, where ζ and A are the thickness and absorbance of the analyzed photocatalyst, respectively, υ is the photon's frequency, and A^* is a constant. The n factor depends on the nature of electron transition and can be equal to ½

or 2 for the indirect or direct transition band-gaps respectively. To apply the Tauc method, the optical absorbance data of the photocatalysts were plotted as a function of the incident photon energy.

2.4. Measurement of the irradiation intensity of the used photonic sources

The radiant sources used to perform the photocatalytic CO_2 reduction using Co/TiO_2 photocatalysts, were the following: (i): a short-wave Hach UV lamp (254 nm), (ii) 60-watts and 100-watts lamps (600 nm), and (iii) 14-watts led spotlight (600 nm). The UV radiation intensity of the photonic sources was measured using an UVX model UVP radiometer, equipped with three interchangeable sensors to determine different UV wavelengths: short wavelength (254 nm, UVc), medium wavelength (310 nm, UVb), and long wavelength (360 nm, UVa). The total irradiation of the visible photonic sources was determined using a MacSolar pyrheliometer, with an irradiant intensity detection between 0 and 1500 W/m^2.

2.5. Photocatalytic CO_2 reduction

Photocatalytic CO_2 reduction reactions were performed in a batch reactor, with an effective volume of 1 L, made of Pyrex-glass provided with a quartz-window, that allows light radiation to pass through. The CO_2 photoreduction system is shown in Fig. 1. The reaction conditions were as follows: 100 ml of distilled water as electron donor agent and 10 g of photocatalyst were deposited into the reaction system. A 100 ml/min CO_2 gas flow (99.98% INFRA) was bubbled in the water contained in the reactor for 15 min, to remove the air out of the reactor and to dissolve CO_2 in the water. The reaction conditions were adjusted to atmospheric pressure at 30 ± 2 °C. The reactor was illuminated using the different radiant sources for 1 h.

After one hour of irradiation, a 10 ml gas sample was extracted by entrainment with CO_2 bubbling in the liquid phase at flow rate of 10 ml/min and analyzed by Fourier Transform Infrared (FTIR) spectroscopy using a Bruker Vertex 70 model spectrophotometer. The sample was analyzed using 150 scans in Attenuated Total Reflectance (ATR) mode with a resolution of 4 cm^{-1}. The reference gas used was Helium (INFRA 99.99%). The quantitative determination of the products formed was estimated using the Grams/AI 7.02 Software.

The stability tests of the photocatalysts, were performed by repeating the process 10 times using the same photocatalyst sample.

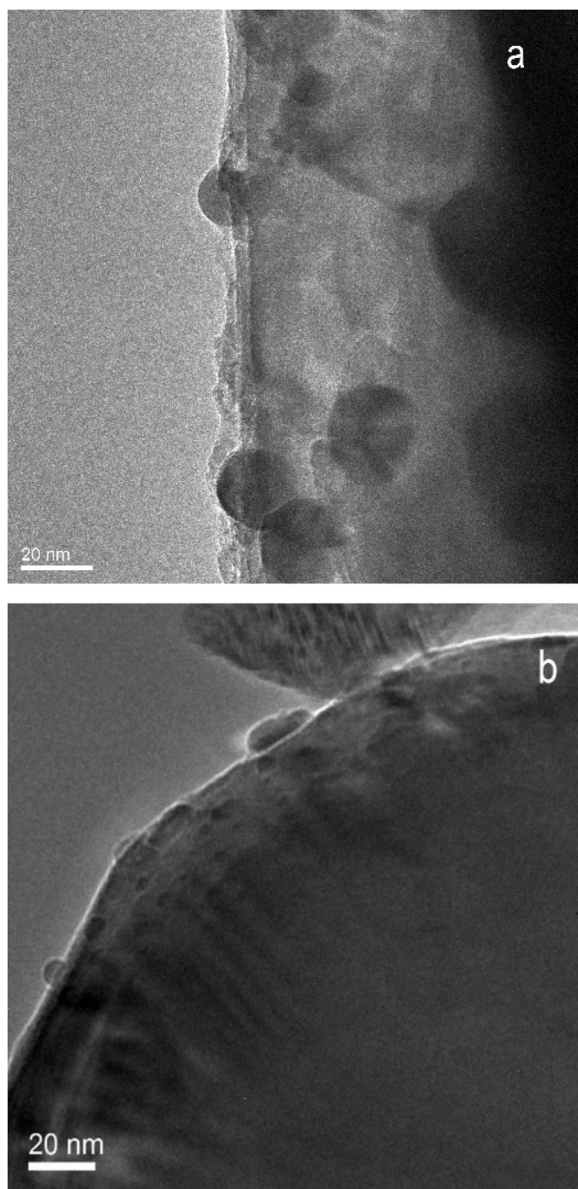The photoreduction quantum efficiency (Φ) (%) for alcohols pro-

Fig. 2. HR-TEM micrographs of photocatalysts: a) 1%Co$_3$O$_4$/TiO$_2$, b) 10% Co$_3$O$_4$/TiO$_2$.

duction was calculated from Eq. 8.

$$\Phi(\%) = \frac{r_{e^-} \cdot Product \text{ formation } rate\left(\frac{mol}{h}\right)}{\text{incident photon } rate\left(\frac{mol}{h}\right)} \bullet 100\% \qquad (8)$$

where r_{e^-} is the number of moles of electrons required to reduce 1 mol of CO$_2$ to 1 mol of a desired alcohol [40].

The incident photon rate can be calculated by Eq. 9 [41].

$$\text{incident photon } rate = \frac{I(W/m^2) \bullet A(m^2)}{h(J \bullet s) \bullet c(m/s)/\lambda(m)} \qquad (9)$$

where I is the incident light intensity, A is de area of light irradiation projected on the reactor, h is the Planck constant (6.626×10^{-34} J·s), c (2.997×10^8 m·s^{-1}) is the speed light and λ is the wavelength of the light (600 nm).

The alcohols selectivity was calculated using Eq. 10.

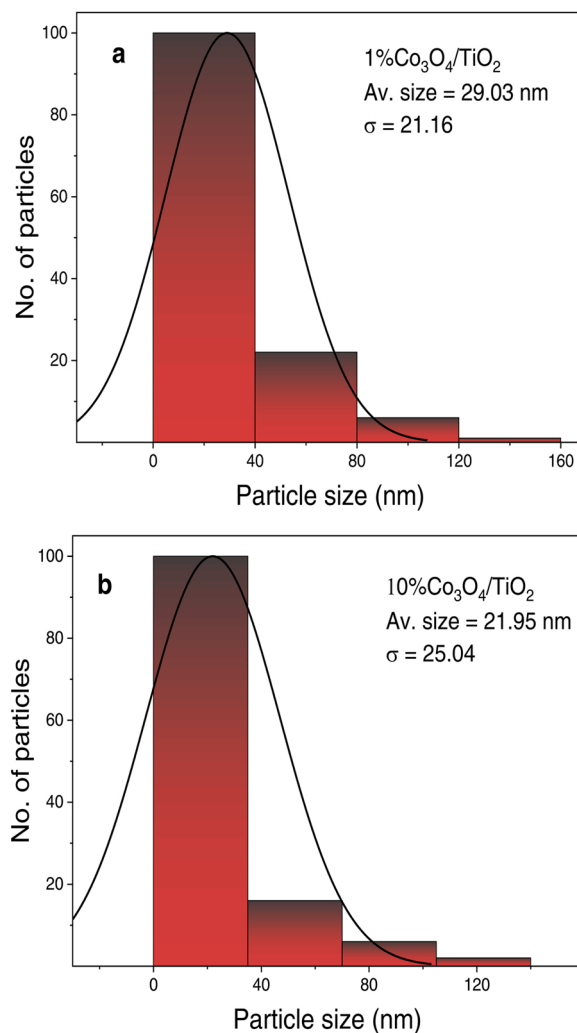$$\text{selectivity}_i = \frac{[especie]_i}{\sum\limits_i^n [especie]_i} \qquad (10)$$

Fig. 3. Cobalt particle size distribution on TiO$_2$ surface: a) 1%Co$_3$O$_4$/TiO$_2$, b) 10% Co$_3$O$_4$/TiO$_2$.

Table 2
Photocatalysts characterization data.

Photocatalyst	d$_{Co}$ (nm)	D$_{Co}$ (%)	Number of total Co atoms·g$_{cat}^{-1}$	Number of surface Co atoms·g$_{cat}^{-1}$
1%Co$_3$O$_4$/ TiO$_2$	29.03	3.15	1.02×10^{20}	3.22×10^{18}
10%Co$_3$O$_4$/ TiO$_2$	21.98	4.17	10.21×10^{20}	42.50×10^{18}

3. Results and discussion

3.1. Catalyst characterization

3.1.1. HR-TEM study of the photocatalysts

HR-TEM images of fresh 1%Co$_3$O$_4$/TiO$_2$ and 10% Co$_3$O$_4$/TiO$_2$ are shown in Fig. 2. Formation of spherical shaped cobalt nanoparticles of varying sizes over TiO$_2$ surface can be observed. Fig. 3 shows the cobalt particle size distribution on TiO$_2$ surface. From the images, it can be seen that the particles present a homogeneous size distribution, as most sizes are grouped in the center of the graph. The mean Co particles size (d$_{Co}$) and the cobalt dispersion values (D$_{Co}$), were calculated from HR-TEM images. The number of surface Co atoms in the photocatalysts was calculated from dispersion values. The estimated values are summarized
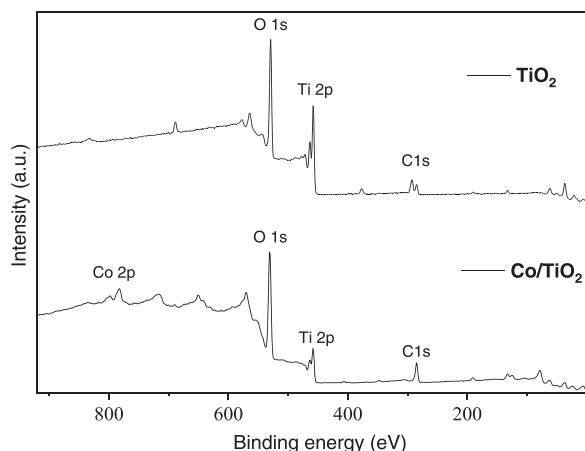
Fig. 4. Survey analysis of photocatalysts.

Table 3
Binding Energy positions of the components and Co/Ti atomic ratio of the photocatalysts. The % peak area of Ti^{4+}, Ti^{3+}, Co^{3+} and Co^{2+} components are presented in parentheses.

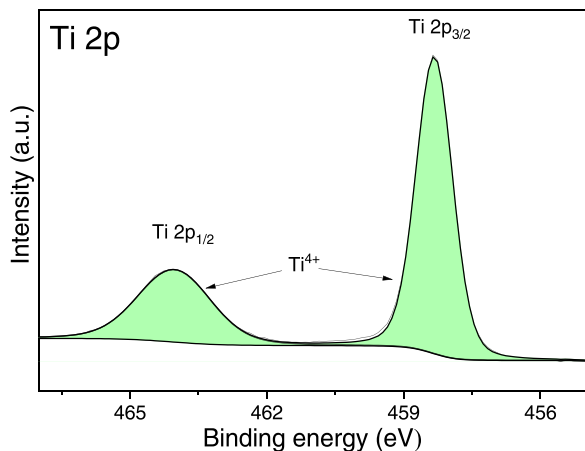| Photocatalyst	Ti $2p_{3/2}$ (eV)	Ti oxidation state	Co $2p_{3/2}$ (eV)	Co oxidation state	Co/Ti atomic ratio
TiO_2	458.08 (100)	Ti^{4+}	—	—	
$1\%Co_3O_4/$ TiO_2	459.75 (33)	Ti^{3+}	780.04 (71)	Co^{3+}	0.27
	458.40 (67)	Ti^{4+}	782.37 (29)	Co^{2+}	

Fig. 5. XPS spectrum of Ti on pure TiO_2.

in Table 2.

3.1.2. X-ray photoelectron spectroscopy characterization of the photocatalysts

XPS analysis was performed on TiO_2 and $1\%Co_3O_4/TiO_2$ photo-catalysts. The survey analysis of pure TiO_2 and $1\%Co_3O_4/TiO_2$ are displayed in Fig. 4. The estimated binding energy (BE) values of Ti $2p_{3/2}$ and Co $2p_{3/2}$ levels and atomic percentages of Co and Ti species in different oxidation states are presented in Table 3.

The high-resolution XPS spectrum of TiO_2 sample, displayed in Fig. 5, revealed two peaks ascribed to Ti $2p_{3/2}$ and Ti $2p_{1/2}$ with single components located at the binding energies 458.32 eV and 464.05 eV, corresponding to the valence state of Ti^{4+} ions in TiO_2 [42–45]. As can be seen, these emission bands revealed that Ti is present only as Ti^{4+}.
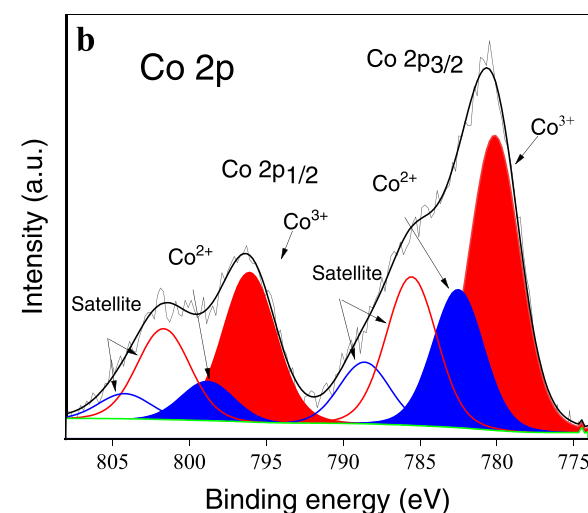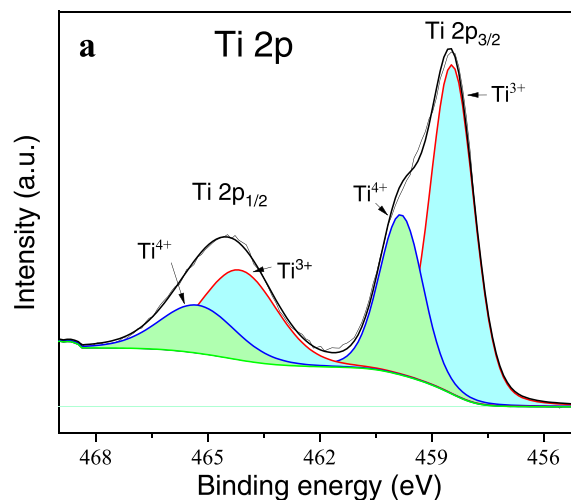

Fig. 6. High-resolution XPS spectrum of a) Ti 2p and b) Co 2p in 1% Co_3O_4/TiO_2.

The high-resolution XPS spectrum of $1\%Co_3O_4/TiO_2$ sample displayed in Fig. 6(a), shows two peaks at 458.57 eV and 464.57 eV ascribed to Ti $2p_{3/2}$ and Ti $2p_{1/2}$ respectively. The Ti 2p components are well deconvoluted into four peaks. The peaks appearing at 458.4 eV and 464.27 eV correspond to Ti^{4+} and the peaks at 459.75 eV and 465.37 eV are assigned to Ti^{3+} electronic state [42–44, 46]. The results suggest that Co presence leads to the generation of the valence state of Ti^{3+} ions at TiO_2 surface. The XPS analysis indicated about 67% Ti^{4+} and 33% Ti^{3+} at the photocatalyst surface.

Fig. 6(b) shows the high-resolution XPS spectrum of the Co 2p component in $1\%Co_3O_4$, which revealed two spin-orbit split lines at 780.68 and 796.48 eV corresponding to Co $2p_{3/2}$ and Co $2p_{1/2}$, respectively, separated by 15.8 eV [47]. The peaks at 782.37 and 780.04 in the Co $2p_{3/2}$ component, can be attributed to Co^{2+} and Co^{3+} oxidation states, respectively. Whereas the peaks at 798.88 eV and 796.08 eV in Co $2p_{1/2}$, can be attributed to Co^{2+} and Co^{3+} oxidation states, respectively [45, 48–50]. Additionally, both Co $2p_{3/2}$ and Co $2p_{1/2}$ components contain their corresponding satellite peaks. These results suggest the presence of oxidized Co, evidencing the interaction between Co atoms and O atoms [48]. The analysis revealed a higher % peak area of Co^{3+} (71%) related to that of Co^{2+} (29%). The XPS estimated Co/Ti ratio in the photocatalyst indicates that about 27% of the Ti surface atoms is covered by cobalt species (Table 3).
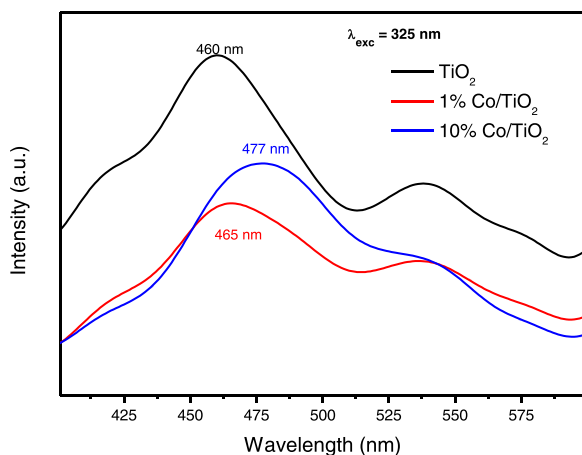
Fig. 7. Photoluminescence emission spectra of the photocatalysts annealed at 900 °C for 4 h.
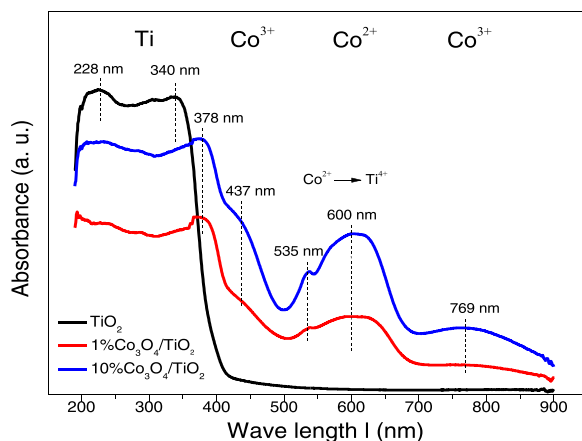

Fig. 8. UV–vis spectra of photocatalysts.

3.1.3. Photoluminescence spectra of the photocatalysts

Fig. 7 represents the photoluminescence spectra of the photocatalysts. As can be seen in the figure, the pristine TiO_2 sample revealed emissions in the 400–600 nm range, with the principal emission peak around 460 nm. However, the position of the principal emission band in the 1%Co/TiO_2 sample, shifted to 465 nm and that in the 10%Co/TiO_2 sample, shifted to 477 nm. Apart from this principal emission band, the emission spectra of all the catalysts revealed one hump at the higher energy side (around 420 nm) and one low-intensity band at the lower energy side (around 538 nm). The characteristics of the emission bands of the photocatalysts are very similar to those of the emission bands in sol-gel Co-doped TiO_2 nanoparticles reported by Choudhury et al. [51]. While the hump appeared around 420 nm has been associated with self-trapped excitons (STE), localized on TiO_6 octahedra, the bands that appeared around 460 and 538 nm, have been associated with oxygen vacancies.

As can be noticed, the emission bands in the Co-incorporated TiO_2 samples, clearly indicates a reduction of charge-carrier recombination due to the formation of trap-states at the band-gap of TiO_2 or formation of heterostructure between TiO_2 and Co_3O_4, reducing the rate of electron-hole recombination. A reduction of the recombination rate of the photogenerated charge carriers in the system, also enhances the carrier lifetime. As the intensity of emission in the 1%Co/TiO_2 photocatalyst is lower than that in the 10%Co/TiO_2 photocatalyst, the carrier lifetime in the earlier sample is expected to be longer than in the latter (10%Co/TiO_2) sample.

Table 4

Band gap energy of the photocatalysts estimated according to Planck's equation.

Photocatalysts	E_g (Planck's equation) (eV)		
	Ti^{4+}	Co^{2+}	Co^{3+}
TiO_2	2.97		
1%Co_3O_4/TiO_2	2.72	1.65	1.93
10%Co_3O_4/TiO_2	2.61	1.71	2.24

Table 5

Band gap energy of photocatalysts estimated according to Tauc method.

Photocatalyst	E_g (Tauc method) (eV)					
	Direct transitions			Indirect transitions		
	Ti^{4+}	Co^{2+}	Co^{3+}	Ti^{4+}	Co^{2+}	Co^{3+}
TiO_2	3.20			2.98		
1%Co_3O_4/TiO_2	2.91	1.80	2.47	2.78	1.78	2.19
10%Co_3O_4/TiO_2	2.85	1.85	2.51	2.59	1.75	2.31

3.1.4. Diffuse reflectance spectra of the photocatalysts

To investigate the effect of cobalt addition on TiO_2 photoactivity for CO_2 photoreduction, 1%Co_3O_4/TiO_2, and 10%Co_3O_4/TiO_2 photocatalysts were prepared and characterized by their UV-Vis diffuse reflectance spectra, measured in diffuse reflectance mode in the UV-Vis spectral range (Fig. 8). In these spectra, the following facts can be observed.

TiO_2 exhibited strong optical absorption in the UV range appearing between about 400–200 nm. This absorption band is attributed to the charge transfer from TiO_2 valence band, formed mainly by the 2p orbitals of the oxide anions (O^{2-}) to the conduction band, formed by the 3d t_{2g} orbitals of the Ti^{4+} cations [52].

It can be observed in Co/TiO_2 spectra, a red-shift of the absorption band of TiO_2. Therefore, a decrease in the TiO_2 band-gap value was measured. This fact can be attributed to the presence of cobalt in the TiO_2 surface, that modifies its band structure at the interface and forms additional absorption bands near the Fermi level of TiO_2 [22,53]. It can also be observed that presence of Co in TiO_2, generated new absorption bands in the visible region, between 415 and 850 nm.

According to Chen et al. [54] the absorption bands between 535 and 700 nm over Co/TiO_2 spectra, can be attributed to the $^2E(G)$, $^4T_1(P)$, $^2A_1(G)\rightarrow$ ground state $^4A_2(F)$ transition for high-spin Co^{2+} ($3d^7$) in tetrahedral coordination. On the other hand, Qu et al. [55], suggested that the bands observed around 535 and 610 nm are owing to the crystal field splitting, the band $3d^7$ associated with Co^{2+} ions splitting into two sub-bands, which are called $Co^{2+}\rightarrow Ti^{4+}$ charge-transfer bands.

The absorption bands at 437 nm and 739 nm over Co/TiO_2 can be assigned to $^1A_{1g} \rightarrow {}^1T_{2g}$ and $^1A_{1g} \rightarrow {}^1T_{1g}$ transitions of Co^{3+} ions in octahedral symmetry. These results show that both ions (Co^{2+} and Co^{3+}) are present at the surface of Co/TiO_2 photocatalysts [54].

The band gap energies of the photocatalysts were calculated by Planck's equation, determined by intercepting a straight line fitted in the linear region of the spectrum with the wavelength axis (Fig. S1, Supplementary Material). The estimated E_g values are reported in Table 4. It can be seen for Co/TiO_2 catalysts, that addition of Co to TiO_2 resulted in a lowering of its band gap energy. It can also be observed that the decrease in band gap energy was higher for 10% Co_3O_4/TiO_2 than for 1%Co_3O_4/TiO_2.

The Tauc method was used to calculated Eg values for direct (n = 2) (Fig. S2) and indirect transitions (n = 1/2) (Fig. S3), according to Eq. 7. In Table 5, the band-gap estimations using the Tauc method have been reported. In this table, TiO_2 band gap energy values of 3.20 eV and 2.98 eV, can be observed, corresponding to allowed direct and indirect transitions respectively. These values, suggest that TiO_2, calcined at

Table 6

UV radiation intensity of photonic sources.

Source	UV radiation intensity ($\mu W/cm^2$)			Total visible radiation intensity (W/m²)
	360 nm	310 nm	250 nm	
100-watt light bulb	17.3	3.5	3.2	364
60-watt light bulb	14.2	3.5	3.0	328
14-watt led spotlight	2.1	1.5	1.6	122
UV lamp	56.2	51	1070	—

900 °C, is composed mainly of rutile phase. The assumption is supported by Tobaldi et al. [56], who determined, (in a study of TiO_2, calcined at 800 °C, using the Tauc method), a band gap energy value of 3.07 eV for the direct allowed transition and 2.91 eV for indirect allowed transition.

In Table 5, it can be seen, for $1\%Co_3O_4$ and $10\%Co_3O_4/TiO_2$ photocatalysts, that addition of Co to TiO_2 resulted in a lowering of its band gap energy values, for direct and indirect transitions. It can also be observed that the decrease in the band gap energy was higher for 10% Co_3O_4/TiO_2 than for $1\%Co_3O_4/TiO_2$. The difference in band-gap energy decrease may be due to the higher number of Co surface atoms interacting with TiO_2 in $10\%Co/TiO_2$ than in $1\%Co_3O_4/TiO_2$, as determined from HRTEM analysis (Table 2). These results, are in agreement with Song et al. [57] who reported for TiO_2, in calcined Co/TiO_2 photocatalyst, a band gap energy of 2.72 eV, which is lower than that of pristine TiO_2 (3.10 eV). The red-shift of the band, was explained, considering electronic transitions from the TiO_2 valence band to the Co level or from the Co level to the TiO_2 conduction band.

In the Co/TiO_2 photocatalysts spectra (Fig. 8), it can be seen, a band spanning 500–700 nm, which can be attributed to Co^{2+} transitions, as was suggested by G. et al. [58] and Xiuhua et al. [59], who studied a calcined Co/TiO_2 photocatalyst. These authors report, for the catalyst UV-Vis spectrum, an absorption band in the visible region from 610 nm to 700 nm, corresponding to Co^{2+}. In the spectra shown in Fig. 8, it can be seen for Co/TiO_2 catalysts, a band spreading between 700 and 900 nm, and a small shoulder appearing between about 425 and 480 nm. Both bands can be associated to $O^{2-} \rightarrow Co^{3+}$ transition.

3.2. Photonic intensities estimation

In Table 6, the different UV radiation intensities estimated for the UV and visible light sources used to investigate the photocatalytic process are reported. As can be seen, 100-watt, 60-watt and 14-watt visible light lamps, also emitted UV radiation. In the table, it can also be observed, the values of the total irradiation intensity measured inside the photoreactor, using the visible photonic sources.

3.3. Photocatalytic CO_2 reduction with H_2O

To evaluate the effect of radiation energy, on CO_2 photoreduction accelerated by TiO_2, $1\%Co_3O_4/TiO_2$ and $10\%Co_3O_4/TiO_2$, four different photonic radiation sources were used (Table 6). The effect of Co loading in Co/TiO_2 photocatalysts for CO_2 photocatalytic reduction was also investigated. The photocatalysts were prepared with two different cobalt concentrations: $1\%Co_3O_4/TiO_2$ and $10\%Co_3O_4/TiO_2$. After 1 h of irradiation, the gas samples were obtained by bubbling CO_2 in the reaction liquid phase. These samples may contain the molecules of the products dissolved in the reaction medium and the molecules of the volatile products entrained by the CO_2 flow. The gas samples were analyzed by FTIR spectroscopy.

A blank reaction was performed, without the photocatalyst, under similar reaction conditions (2.5 Photocatalytic CO_2 reduction). For this reaction, no product formation was detected under any of the radiation sources.

Table 7

Products detected by FTIR spectroscopy, during photocatalytic CO_2 reduction with H_2O, catalyzed by TiO_2, $1\%Co_3O_4/TiO_2$ and $10\%Co_3O_4/TiO_2$, using UV lamp as radiation source.

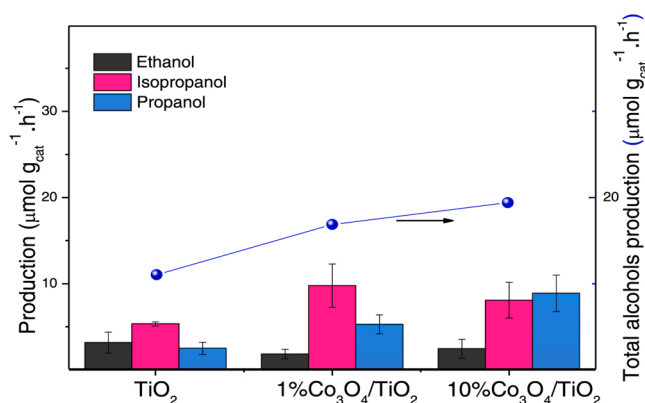| Products ($\mu mol/g_{cat} \cdot h$)	Photocatalyst		
	TiO_2	$1\%Co/TiO_2$	$10\%Co/TiO_2$
Carbon monoxide	0.19	0.20	0.16
Hydrogen peroxide	0.45	0.28	0.41
Formic acid	0.01	0.01	0.01
Acetone	0.17	0.16	0.14
Acetaldehyde	0.01	0.09	0.09
Formaldehyde	0.01	0.01	0.01
Propionaldehyde	0.01	0.01	0.01
Methanol	0.01	0.01	0.01
Ethanol	3.16	1.83	2.44
Isopropanol	5.32	9.76	8.07
Propanol	2.49	5.27	8.87

Fig. 9. Ethanol, isopropanol, and propanol production on TiO_2-based photocatalysts under UV irradiation.

In Table 7, the results of the quantitative analysis of the gas samples are presented for CO_2 photoreduction during irradiation with UV light using TiO_2, $1\%Co_3O_4/TiO_2$ and $10\%Co_3O_4/TiO_2$ as photocatalysts and Fig. 9 shows the distribution of the detected main products: ethanol, propanol and isopropanol. In the figure, it can be seen that during UV irradiation, $1\%Co_3O_4/TiO_2$ and $10\%Co_3O_4/TiO_2$ presented higher activities than that of TiO_2 for isopropanol and propanol production, suggesting a promotional effect of Co on TiO_2 photoactivity under UV irradiation. In the figure, it can be seen that a small activity of the three catalysts for ethanol production was measured.

The photocatalytic activity of TiO_2 irradiated with UV light for methanol production through CO_2 photoreduction, has been studied by Wang et al. [60]. On the other hand, Olivo et al. [61] showed that the CO_2 photoreduction catalyzed by TiO_2, at high H_2O/CO_2 molar relation, generated peroxocarbonate species, which are further reduced to formic acid, formaldehyde and methanol. This reaction route is explained, assuming that the CO_2 hydrogenation rate is higher than its deoxygenation rate, leading to the formation of oxygenated hydrocarbons. On the other hand, Spadaro et al. [20], using Cu/TiO_2 as photocatalyst, for CO_2 photoreduction with H_2O, detected formaldehyde, acetaldehyde and ethanol production. The authors suggested that the CO_2 photoreduction process in water involved a variable reaction network, due to the large number of possible reactions and of electrons transferred between photogenerated carriers and species within the reaction system.

The absorption spectra of $1\%Co_3O_4/TiO_2$ and $10\%Co_3O_4/TiO_2$ in the UV–vis spectral range, shown in Fig. 8, revealed strong absorption band spanning 400–800 nm corresponding to Co^{2+} and Co^{3+} absorption in the visible region. The increase of TiO_2 photocatalytic activity in presence of Co, can be explained, considering the increase in the recombination time of the excited electrons in the conduction band of TiO_2 as

Table 8

Products detected by FTIR spectroscopy, during photocatalytic CO_2 reduction with H_2O, catalyzed by TiO_2, $1\%Co_3O_4/TiO_2$ and $10\%Co_3O_4/TiO_2$, under 328 W/m^2, using visible lamp as radiation source (60-watt light bulb).

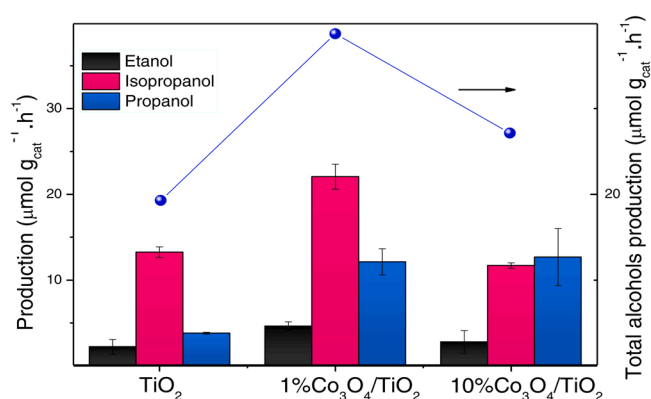| Products ($\mu mol \cdot g_{cat} \cdot h$)	Photocatalyst		
	TiO_2	$1\%Co/ TiO_2$	$10\%Co/ TiO_2$
Carbon monoxide	0.41	0.30	0.13
Hydrogen peroxide	0.65	0.61	0.39
Formic acid	0.01	0.01	0.01
Acetone	0.04	0.15	0.09
Acetaldehyde	0.12	0.49	0.02
Formaldehyde	0.01	0.01	0.03
Propionaldehyde	0.01	0.05	0.05
Methanol	0.03	0.01	0.03
Ethanol	2.22	4.63	2.71
Isopropanol	13.26	22.05	11.70
Propanol	3.80	12.12	12.67

Fig. 10. Ethanol, isopropanol, and propanol production on TiO_2-based photocatalysts under visible radiation (60-watts light bulb, 328 W/m^2).

proposed by Kumar Singh et al. [62] and Usubharatana et al. [63]. The highest production of isopropanol under UV irradiation was detected from the photocatalyzed CO_2 reduction with H_2O, using $1\%Co_3O_4/TiO_2$ as photocatalyst, while the highest propanol production was detected when the reaction was photocatalyzed by $10\%Co_3O_4/TiO_2$.

In Table 8, the results of the quantitative analysis of the gas samples are presented for CO_2 photoreduction during visible irradiation with a 60-watts light bulb (328 W/m^2), using TiO_2, $1\%Co_3O_4/TiO_2$ and 10% Co_3O_4/TiO_2 as photocatalysts and Fig. 10 shows the distribution of the detected main products: ethanol, propanol and isopropanol. The figure shows that TiO_2 presented lower activity related to that of $1\%Co_3O_4/$ TiO_2 and $10\%Co_3O_4/TiO_2$. However, $1\%Co_3O_4/TiO_2$ manifested the highest photocatalytic activity, generating about 5, 22, and 12 $\mu mol/$ $g_{cat} \cdot h$ for ethanol, isopropanol and propanol respectively.

The results presented are in agreement with Ola et al. [64] who reported methanol and ethanol photocatalytic production, using V, Cr, and Co deposited on TiO_2 as photocatalysts and visible light as radiation source. These authors reported that the optimum methanol and ethanol production was attained using $1\%Co_3O_4/TiO_2$ as photocatalyst. The results shown in Figs. 9 and 10 demonstrate the crucial effect of photon energy in the photoreduction reaction of CO_2 with H_2O.

The total alcohols production was higher when it was photocatalyzed by $1\%Co_3O_4/TiO_2$ than by $10\%Co_3O_4/TiO_2$. This result can be explained considering that increased electron-hole recombination rate may increase, with higher Co concentration, due to increased Co^{2+} and Co^{3+} species, which act as electron or hole traps, increasing the electron-hole recombination probability, as it has been reported in the literature [65, 66].

On the other hand, a probable cause of the reduced photoactivity of $10\%Co_3O_4/TiO_2$ related to that of $1\%Co_3O_4/TiO_2$ can be attributed to

Table 9

Factorial design matrix for CO_2 photoreduction with H_2O.

Run	Natural factors		Coded factors		Total response	
	Co concentration (%)	Irradiance intensity (W/m^2)	A	B	Total alcohols production ($\mu mol/g_{cat} \cdot h$)	
1	0	122	-1	-1	7.657	7.823
2	1	122	0	-1	19.530	19.030
3	10	122	1	-1	26.576	27.131
4	0	328	-1	0	25.189	26.243
5	1	328	0	0	37.062	40.557
6	10	328	1	0	22.137	21.804
7	0	364	-1	1	22.637	24.190
8	1	364	0	1	23.580	30.626
9	10	364	1	1	26.465	21.693

the higher coverage of TiO_2 surface with increased Co ions in 10% Co_3O_4/TiO_2, which can strongly reduce interfacial charge transfer between Co species and TiO_2. This suggestion is supported by the number of surface Co atoms/g photocatalyst values estimated for the photocatalysts. As can be seen in Tables 2, $1\%Co_3O_4/TiO_2$ presented a strongly lower number of surface Co atoms/g photocatalyst (3.22×10^{18}) than $10\%Co_3O_4/TiO_2$ (42.50×10^{18}).

In Tables S1 and S2 (Supplementary Material), the results of the quantitative analysis of the gas samples are presented for photocatalytic CO_2 reduction during visible irradiation with a 14-watt light bulb (122 W/m^2), and with a 100-watt light bulb (364 W/m^2) respectively. The tables show that using these radiation sources resulted in lower amounts of all the products for photocatalytic CO_2 reduction compared to those generated using a 60-watt light bulb (328 W/m^2).

In order to determine the stability of the photocatalysts, recycling tests over TiO_2, $1\%Co_3O_4/TiO_2$ and $10\%Co_3O_4/TiO_2$ were performed. The ethanol, propanol and isopropanol yield as a function of the number of photocatalytic CO_2 reduction cycles under UV and visible (60-watts light bulb) irradiation are presented in Figs. S4, and S5 (Supplementary Material) respectively. In these figures, it can be seen that even after 10 cycles, the activity of the photocatalysts remained almost unaltered, indicating a strong stability during the photocatalytic CO_2 reduction under UV and visible irradiations.

3.4. CO_2 photoreduction test on visible irradiance function and cobalt concentration via design of experiments (DOE)

To deepen the investigation on the photocatalytic CO_2 reduction with H_2O using TiO_2, $1\%Co_3O_4/TiO_2$ and $10\%Co_3O_4/TiO_2$ photocatalysts, we evaluated the combined effects of cobalt concentration and the intensity of the luminous irradiance generated by the different visible-light sources used in this study, on the evolution of total alcohols production. The evaluation was performed following a 3^2-factorial design of experiments (DOE). The factorial design independent variables considered for the evaluation are: Factor A, which is the concentration of cobalt deposited on the TiO_2 surface (0 wt%, 1 wt%, and 10 wt%) in the low, medium, and high levels. The codified variables of the concentrations are -1, 0, and $+1$ respectively; Factor B is the intensity of irradiance on the illuminated surface, inside the reactor: 122, 328, and 364 W/m^2 corresponding to 14-watt led spotlight, 60-watt light bulb and 100-watt light bulb respectively, in the low, medium, and high levels. The codified variables of the intensities are -1, 0, and $+1$ respectively.

As a response variable, the total μmoles of the produced alcohols during 1 h of reaction was calculated. Table 9 presents the experimental design matrix with the coded factors and the response variables.

The data obtained from the development of the design of experiments were applied to calculate the yield, the quantum efficiency and the selectivity, for each of the main products (ethanol, isopropanol and

Table 10

CO_2 photoreduction yields over different reaction conditions.

Run	Product yield ($\mu mol \cdot g_{cat}^{-1} \cdot h^{-1}$)		
	C_2H_5OH	iC_3H_7OH	C_3H_7OH
1	1.997	3.551	2.192
2	3.107	9.931	12.678
3	1.970	8.239	13.205
4	2.219	13.260	3.801
5	4.633	22.054	12.123
6	2.719	11.707	12.678
7	4.494	10.930	11.429
8	2.108	6.380	13.482
9	2.580	6.713	14.786

Table 11

CO_2 photoreduction activities over different reaction conditions.

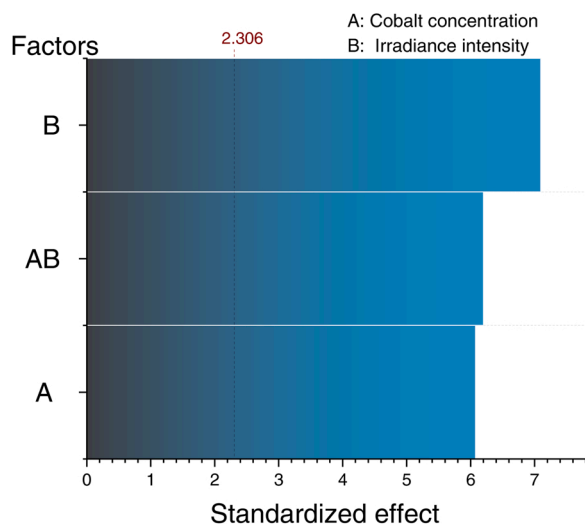| Run	Quantum efficiency (%)			Selectivities (%)		
	C_2H_5OH	iC_3H_7OH	C_3H_7OH	C_2H_5OH	iC_3H_7OH	C_3H_7OH
1	0.041	0.109	0.068	28.80	45.88	28.32
2	0.064	0.306	0.390	12.08	38.62	49.30
3	0.040	0.254	0.407	8.41	35.19	56.40
4	0.017	0.152	0.044	11.51	68.78	19.71
5	0.035	0.253	0.139	11.94	56.83	31.240
6	0.021	0.134	0.145	10.03	43.19	46.78
7	0.031	0.113	0.118	16.74	40.70	42.56
8	0.015	0.066	0.139	9.59	29.04	61.37
9	0.018	0.069	0.153	10.71	27.88	61.41

Fig. 11. Pareto Charts for cobalt concentration and irradiance on total alcohols production from DOE tests.

propanol).

Table 10 shows the results of the calculated yields. In the table, it can be seen that the cobalt concentration has a significant effect on the obtained amounts of the main products. When $1\%Co_3O_4/TiO_2$ photocatalyst is used, the yields of ethanol and isopropanol were highest. However, $10\%Co_3O_4/TiO_2$ generated the highest yield of propanol, in the same photoreaction conditions.

Table 11 shows the results of the quantum efficiency and selectivity in the photoreduction of CO_2. It can be seen that, the quantum efficiency (calculated using Eq. 8) of the main products, deceased as the irradiation intensity increased. The selectivity calculated using Eq. 10 for the main products, evolved similarly as the measured yield, i.e., the selectivity of ethanol and isopropanol decreased with the increase in the concentration of cobalt in the photocatalyst. The selectivity estimations revealed
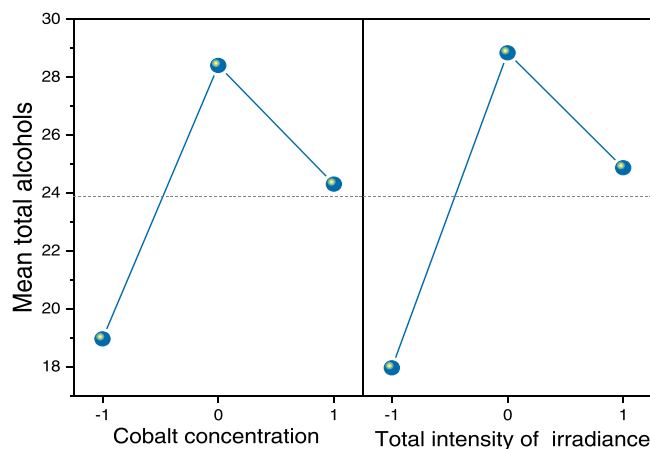

Fig. 12. Main effects plot of cobalt concentration and total intensity irradiance on total alcohols production.
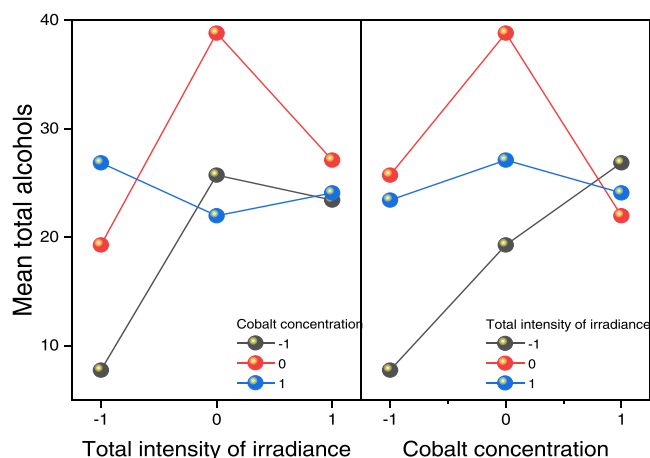

Fig. 13. Combined-effects plot of cobalt concentration and total intensity of irradiance on total alcohols production.

that the medium level of irradiation intensity (328 W/m^2) is the optimal level for the highest selectivity of these photoreduction products. On the other hand, the selectivity of propanol increased with increasing cobalt concentration and with irradiation intensity.

The total concentration of produced alcohols was the sum of the concentrations of ethanol, isopropanol and propanol measured during each run carried out in the design of experiments. The data obtained of the total concentration of alcohols in the photoreduction of CO_2 was statistically analyzed using the statistical Minitab® software 21.1 version. The results reported in the Pareto Charts (Fig. 11) show standardized effects for both variables. Both factors (Co concentration and irradiation intensity) have a statistically significant effect on total alcohols production. In Fig. 11, it can be observed an AB interaction effect, indicating that both variables are dependent on each other.

The main effects plot (Fig. 12) showed the strong effect of cobalt concentration and total intensity of irradiation on the total alcohols production, being the medium point of each analyzed factor, the optimal values in the studied interval proposed for the highest alcohols production from the CO_2 photoreduction with H_2O.

The combined-effects plot (Fig. 13) showed that the highest production of total alcohols is found in the intermediate levels of both factors, and then decreases in the high levels, i.e., there is a curvature effect on the alcohols production from CO_2 photoreduction with H_2O process, as a function of cobalt concentration and irradiance intensity. This effect can be explained considering the interaction of two
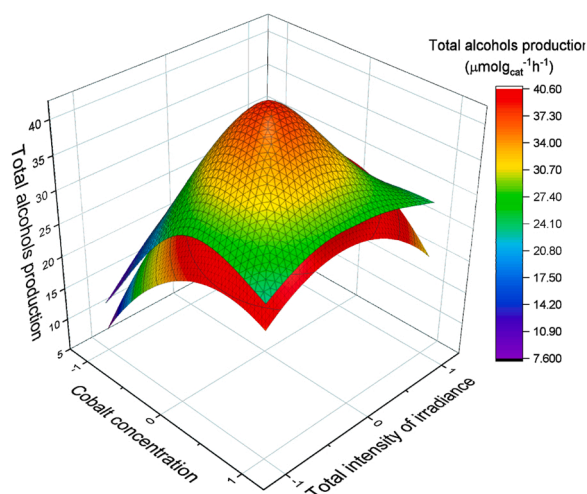
Fig. 14. Response surface on total alcohols production.

phenomena: 1) the formation of additional recombination sites, and 2) the increase in the rate of charge recombination. This assumption was mentioned by Ola et al. [64], who concluded that a too strong doping, induces additional formation of charges recombination centers. On the other hand, Olivo et al. [67] mention that only a fraction of the radiant flux is necessary to activate all the available photocatalytic sites, therefore, an increase in this flux does not provide an increase in the formation of products. Herrmann [68] mentioned that the formation of products at low irradiances is proportional to the input photon flux, while high irradiance values could increase the recombination rate. In other words, there are optimal Co surface concentrations combined with optimal irradiation intensity for the desired alcohols generation.

With the purpose of modelling the process for obtaining alcohols from CO_2 photoreduction with H_2O, a regression analysis was performed to describe the evolution of the total alcohols concentration through a mathematical model based on the factors evaluated.

Fig. 14 shows the response surface in the obtention of total alcohols and the fit of the second-order model to the experimental data (Eq. 11).

$$T.A. = 33.45 + 3.45x + 2.67y - 7.42x^2 - 4.61xy - 6.77y^2 \qquad (11)$$

where T.A. is the total alcohols production in $\mu mol/g_{cat} \cdot h$, x is cobalt concentration and y is the total intensity of irradiance, The goodness of fitting, of the model was calculated from the coefficient of determination ($R^2 = 0.72$) and, the root mean square error (RMSE), calculated from Eq. 12, which shows the difference between the predicted values and the observed values of the model.

$$RMSE = \sqrt{\frac{1}{N}\sum_{i=1}^{N}(predicted - observed)^2} = 4.11 \qquad (12)$$

In regression analysis of variance, the f statistic allows to decide if there is a significant relationship between the dependent variable and the independent variables. Since our statistical value F is greater than the critical value F (prob>F), we can conclude that there is a significant relationship between the dependent variable and the independent variables, as can be seen in Table S3 (Supplementary Material).

3.5. Mechanistic considerations

The XPS and UV–vis spectroscopic analysis of the Co/TiO_2 photocatalysts revealed that cobalt is in the Co^{2+} and Co^{3+} oxidation states. These oxidation states might indicate the presence of CoO and Co_3O_4. Now, it is well known that the Co_3O_4 stoichiometric molecular composition is $(Co^{2+})(Co^{3+})_2O_4$ [69], which indicates a cobalt species ratio of:

$$Co^{2+}/Co^{3+} = 0.5$$

The XPS analysis results presented in Table 4, revealed for Co/TiO_2 photocatalyst, a ratio of cobalt species % peak-area of:

$$Co^{2+}/Co^{3+} = 29/71 = 0.4$$

which is close to that of cobalt species in Co_3O_4 molecule. This result suggests the presence of mainly Co_3O_4 at the photocatalysts surface.

This assumption is supported by the standard Gibbs' energy of formation (ΔG_f^0) of Co_3O_4 estimated by M. Kale et al. The value is calculated according to the Reaction (1), for a temperature (T) range between 1130 and 1230 K [70].
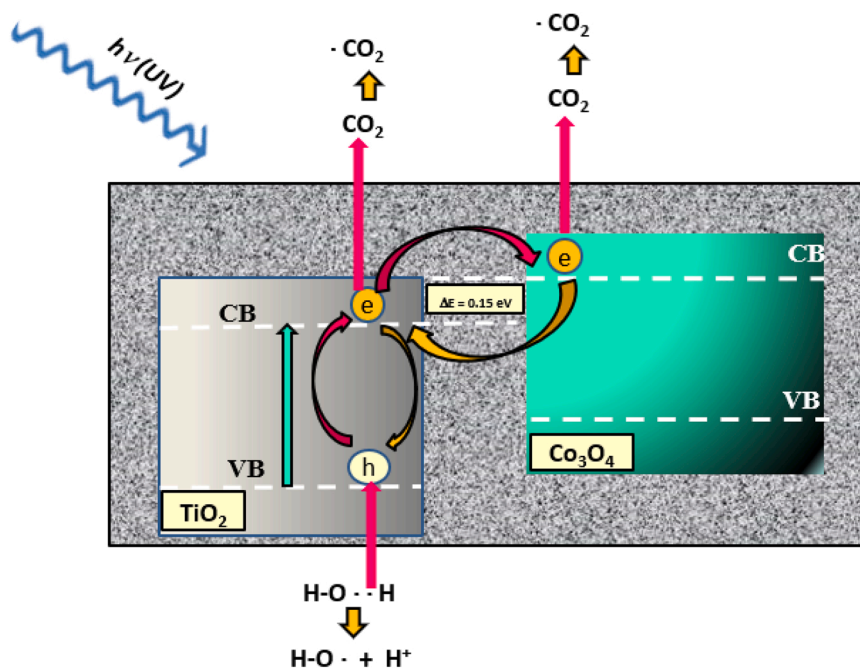

Fig. 15. Schematic presentation of the energy transfer during photocatalytic CO_2 reduction with H_2O, under UV light irradiation, using Co/TiO_2 photocatalysts.
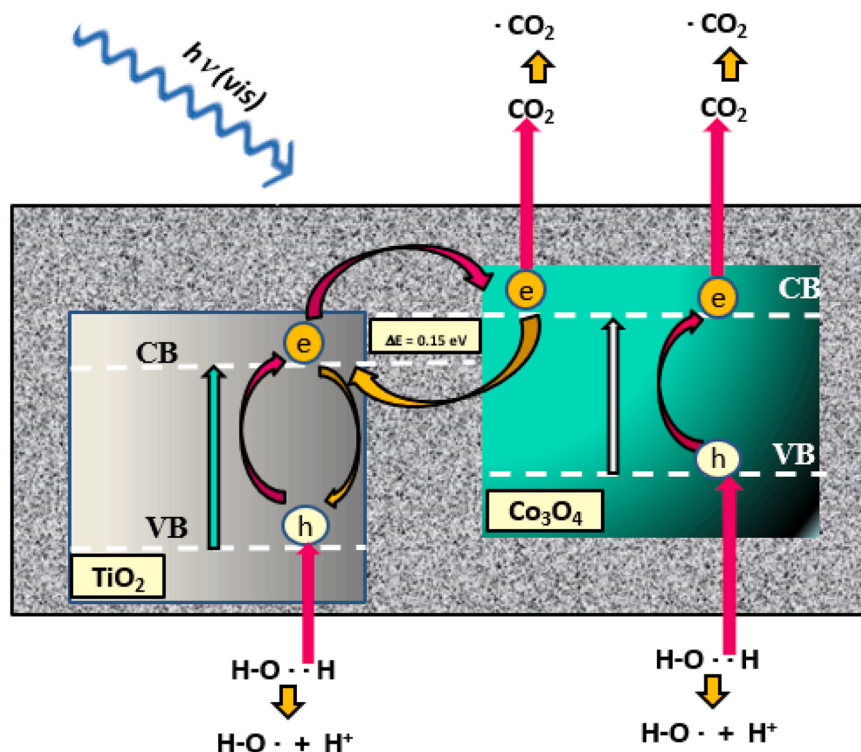
Fig. 16. Schematic presentation of the energy transfer diagram during photocatalytic CO_2 reduction with H_2O photocatalyzed by Co/TiO_2, under visible light.

$$3CoO(s) + 1/2O_2(g) \rightarrow Co_3O_4(s) \tag{R1}$$

$$\Delta G_f^0 = -157,235 Jmol^{-1} + (127.53T)Jmol^{-1}K^{-1} \tag{13}$$

As our photocatalysts were calcined at 900 °C (1173 K), the estimated value for ΔG_f^0 is:

$$\Delta G_f^0 = -42,458 Jmol^{-1} \tag{14}$$

This value indicates that Co_3O_4 formation is spontaneous at 900 °C. Therefore, it is probable that mainly Co_3O_4 may be present at the Co/TiO_2 photocatalysts surface.

Fig. 17. Isopropanol production on TiO_2-based photocatalysts as a function of visible irradiation intensity.

3.5.1. Activity of TiO_2 for photocatalytic CO_2 reduction with H_2O

To explain the effect of energy irradiation and of Co presence, on the activity of TiO_2 for the photocatalytic CO_2 reduction with H_2O, it is convenient to analyze first the results obtained for TiO_2 photocatalyst. As shown in Figs. 9 and 10, the photoactivity of TiO_2 for alcohols production is higher with visible light irradiation using a visible 60-watt light-bulb, than using UV light as radiation source. This fact can be explained, on one hand, considering that UV irradiation leads to higher electron-hole recombination rate than visible light irradiation, leading to lower electron injection to adsorbed CO_2 and to reaction intermediates, thus, resulting in lower photocatalytic reduction rate, as it was demonstrated by Vieira et al. [71]. On the other hand, the fact that TiO_2 manifested photoactivity for CO_2 photoreduction with H_2O under visible light irradiation, with a visible 60-watt light bulb, can be explained, considering the band-gap energy of TiO_2 determined by the Tauc method (for allowed indirect transitions with n = 1/2) which revealed a value of 2.98 eV. This energy corresponds to a wavelength of about 416 nm in the visible region, indicating that TiO_2 electronic transitions can take place during visible light irradiation. Additionally, as can be seen in Table 6, the visible 60-watt light bulb used to irradiate the reaction, emits a small photon flux between 360 nm and 250 nm, corresponding to the UV region. Therefore, this radiation source can additionally activate the absorption bands of TiO_2, in the UV region.

3.5.2. Activity of $1\%Co_3O_4/TiO_2$ and $10\%Co_3O_4/TiO_2$ under UV irradiation

Fig. 9 shows that using $1\%Co_3O_4/TiO_2$ and $10\%Co_3O_4/TiO_2$ as photocatalysts for CO_2 reduction, during one hour, under UV irradiation, resulted in higher alcohols production than using TiO_2. This result indicates that presence of Co at TiO_2 surface resulted in an increase of TiO_2 photoactivity. This result can be explained in basis of the XPS analysis results, which revealed the presence of Ti^{3+}, at the TiO_2 surface in $1\%Co_3O_4/TiO_2$ and $10\%Co_3O_4/TiO_2$. The presence of Ti^{3+} may have enhanced the charge transfer across TiO_2/reactants interface [72], resulting in an increase in the charge transfer to CO_2, H_2O and to the reaction intermediates.
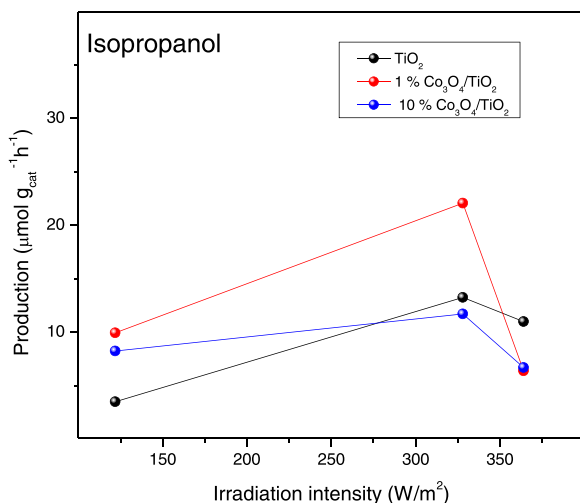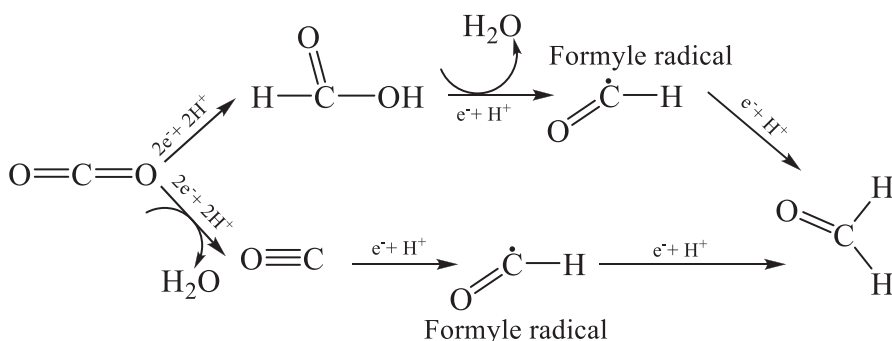
The effect of UV irradiation on photocatalytic CO_2 reduction with H_2O, photocatalyzed by 1%Co/TiO_2, and 10%Co/TiO_2 can be understood from the schematic energy transfer diagram presented in Fig. 15.

Under UV irradiation, electron-hole pairs are generated in TiO_2. The photogenerated electrons will reach the energy state of its conduction band. These electrons can fall down to TiO_2 valence band and recombine with the photogenerated holes, or move to the acceptor levels of the conduction band of Co_3O_4.

This movement would be easily performed by the free electrons of the TiO_2 conduction band, as the Co_3O_4 conduction band lies only about 0.15 eV above the conduction band of TiO_2 [73]. The transferred electrons in the Co_3O_4 conduction band may easily move back to TiO_2 conduction band, and an equilibrated electron movement between TiO_2 and Co_3O_4 would be created. The different transitions of the photogenerated electrons between TiO_2 and Co_3O_4, in Co/TiO_2 photocatalysts, may lower the electron-hole recombination probability, resulting in an improvement of the electron transfer to CO_2 adsorbed molecules at the photocatalyst surface.

3.5.3. Activity of 1%Co$_3$O$_4$/TiO$_2$ and 10%Co$_3$O$_4$/TiO$_2$ under visible irradiation

As can be seen in Fig. 10, under visible irradiation, 1%Co_3O_4/TiO_2 and 10%Co_3O_4/TiO_2 presented higher CO_2 photoreduction with H_2O activity than TiO_2. The increased photoactivity of 1%Co/TiO_2 and 10% Co/TiO_2 under these conditions, can be explained, considering the following facts. TiO_2 is photoactive for the reaction, under visible light irradiation, and Co_3O_4 not only decreases the electron-hole pair

reaction paths is proposed and described as follow.

1. Transfer of CO_2 and H_2O to the surface of Co/TiO_2 photocatalysts.
2. Adsorption of CO_2 and H_2O on the photocatalyst surface. CO_2 adsorption on the photocatalyst surface would take place by the interaction of the d orbitals present in Ti^{3+}, Co^{2+} and Co^{3+} with the π * orbitals of CO_2. The interaction may debilitate the C=O bond, facilitating its bending and cleavage, and the addition of an electron, according to Figs. 15 and 16·H_2O adsorption may take place through the interaction with TiO_2 and Co_3O_4, as represented Figs. 15 and 16.
3. Photo-absorption by Co/TiO_2 photocatalysts and generation of electrons (e^-) and holes (h^+) at TiO_2 and Co_3O_4.
4. Photo-generated h^+ react with H_2O adsorbed at the photocatalyst surface, producing hydrogen ions (H^+) and (·OH) radicals.
5. The CO_2·radical is generated by the reduction of adsorbed CO_2 reacting with photogenerated e^-.
6. The generated H^+, CO_2·radical and e^- react to form intermediates and final products.
7. Desorption of the final products.
8. Transfer of the final products from the photocatalyst surface to the reacting medium.

Based on the products distribution detected during the photocatalytic CO_2 reduction with water over the Co/TiO_2 photocatalysts, reported in Tables 7 and 8, the following reaction steps are proposed.

Step 1. Carbon monoxide (CO), formic acid (CHOOH) and formaldehyde (CH_2O) formation.

recombination rate, but also presents activity for CO_2 photoreduction with water, leading to the alcohols production. Indeed, the UV–vis spectra of 1%Co_3O_4/TiO_2 and 10%Co_3O_4/TiO_2 shown in Fig. 8, indicates that these catalysts can absorb photons in the electromagnetic visible region, due to Co^{2+} and Co^{3+} present at the photocatalyst surface. Therefore, the photoactivity of 1%Co_3O_4/TiO_2 and 10%Co_3O_4/TiO_2 under visible light, can be considered as the contribution of the photoactivity of both TiO_2 and of Co_3O_4. The schematic energy transfer diagram of photocatalytic CO_2 reduction with H_2O photocatalyzed by 1%Co_3O_4/TiO_2 and 10%Co_3O_4/TiO_2 under visible light, can be seen in Fig. 16.

The effect of visible irradiation on photocatalytic CO_2 reduction with water, photocatalyzed by Co_3O_4/TiO_2, photocatalysts is presented in Fig. 16, showing the generation of electron-hole pairs on TiO_2 and on Co_3O_4. Illuminating with visible radiation, electron-hole pairs are formed over both TiO_2 and Co_3O_4. While the electron-hole pairs generated over both semiconductors can also recombine, a constant supply of free electrons from H_2O oxidation would keep the valence band of TiO_2 and of Co_3O_4 filled. Therefore, there would be a constant production of energetic electrons over the conduction band of TiO_2 and Co_3O_4, available for the reduction of CO_2.

Based on the proposed energy transfer diagrams presented in Figs. 15 and 16, a reaction mechanism, following the Langmuir-Hinshelwood
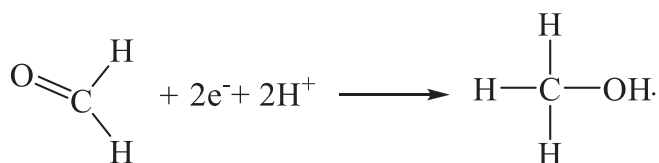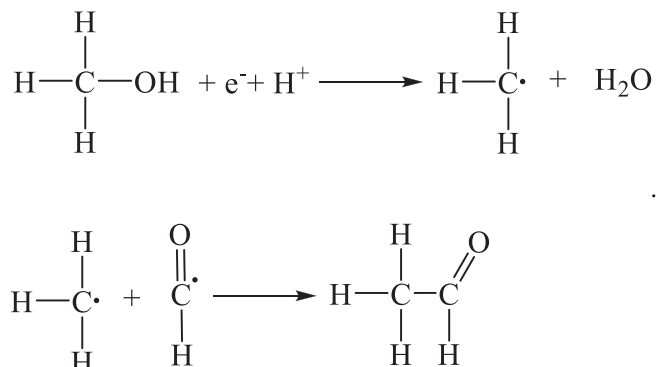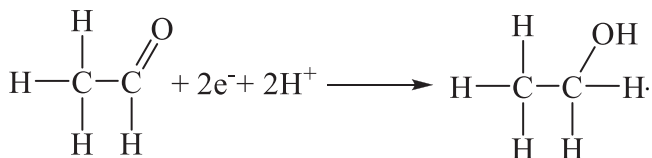
Step 2. Methanol (CH_3OH) formation.

Step 3. Acetaldehyde (C_2H_4O) formation.

Step 4. Ethanol (C$_2$H$_5$OH) formation.

$$H-\underset{\underset{H}{|}}{\overset{\overset{H}{|}}{C}}-\overset{O}{\overset{\|}{C}} + 2e^- + 2H^+ \longrightarrow H-\underset{\underset{H}{|}}{\overset{\overset{H}{|}}{C}}-\underset{\underset{H}{|}}{\overset{\overset{OH}{|}}{C}}-H\cdot$$

Step 5. Propionaldehyde (C$_3$H$_6$O) formation.

$$H-\underset{\underset{H}{|}}{\overset{\overset{H}{|}}{C}}-\underset{\underset{H}{|}}{\overset{\overset{OH}{|}}{C}}-H + \overset{O}{\overset{\|}{\underset{\underset{H}{|}}{C}}}\cdot + e^- + H^+ \longrightarrow H-\underset{\underset{H}{|}}{\overset{\overset{H}{|}}{C}}-\underset{\underset{H}{|}}{\overset{\overset{H}{|}}{C}}-\overset{O}{\overset{\|}{C}} + H_2O$$

.
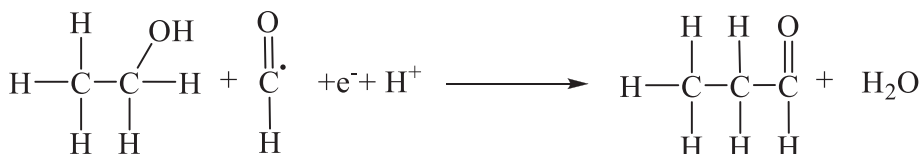
Step 6. Propanol (C$_3$H$_7$OH) formation.

$$H-\underset{\underset{H}{|}}{\overset{\overset{H}{|}}{C}}-\underset{\underset{H}{|}}{\overset{\overset{H}{|}}{C}}-\overset{O}{\overset{\|}{\underset{\underset{H}{|}}{C}}} + 2e^- + 2H^+ \longrightarrow H-\underset{\underset{H}{|}}{\overset{\overset{H}{|}}{C}}-\underset{\underset{H}{|}}{\overset{\overset{H}{|}}{C}}-\underset{\underset{H}{|}}{\overset{\overset{OH}{|}}{C}}-H$$

.
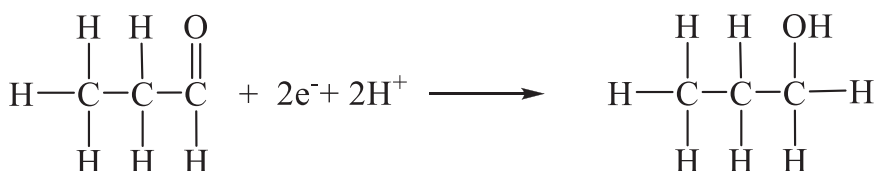
Step 7. Isopropanol (i-C$_3$H$_7$OH) formation.

$$H-\underset{\underset{H}{|}}{\overset{\overset{H}{|}}{C}}-\overset{O}{\overset{\|}{C}} + e^- + H^+ + \cdot CH_3 \longrightarrow H-\underset{\underset{H}{|}}{\overset{\overset{H}{|}}{C}}-\underset{\underset{H}{|}}{\overset{\overset{OH}{|}}{C}}-\overset{\overset{H}{|}}{\underset{\underset{H}{|}}{C}}-H$$

.
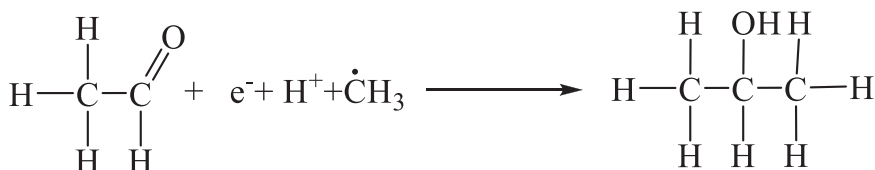
It is interesting to note in Tables 6 and 7, the high concentrations of propanol and isopropanol detected as reaction products. These alcohols are hardly reported in the literature as products, related to the photocatalytic CO$_2$ reduction with H$_2$O. This result can be explained, considering, the production of formyl-radical as it is indicated in Step 1, in which this radical is generated from photocatalytic CO reduction with water. For this step, CO must be adsorbed on the photocatalyst surface. CO adsorption may be strongly enhanced, (as for CO$_2$ adsorption), by the interaction of the multiple electrons of the d orbitals of Ti^{3+}, Co^{2+} and Co^{3+} in the π * orbitals of CO. The described interaction may improve the C≡O bond cleavage, and the addition of photogenerated electrons (e$^-$) and hydrogen-ions (H$^+$).

It can be observed (Step 1), that formyl-radical can also be generated, from formic acid photoreduction. However, Ji et al. in a theoretical study of the mechanism of photoreduction of CO$_2$ to CH$_4$ on TiO$_2$, determined for this reaction, an energy barrier of 2.08 eV, which is much higher than the energy barrier of 1.19 eV determined for CO photoreduction [74]. The result suggests that formyl-radical may have been mainly produced by CO photoreduction. These authors proposed a mechanism in which the rate determining step becomes the photoreduction of CO$_2$ to CO. Accordingly, as our Co/TiO$_2$ photocatalysts may

improve CO$_2$ and CO adsorption rates, its use for photocatalytic CO$_2$ reduction may have improved, first, the CO$_2$ photoreduction to CO (rate determining step), second, the CO photoreduction to formyl-radical, resulting in high generation of the final products (alcohols).

Formyl-radical may have reacted with a methyl-radical to produce acetaldehyde, which may have generated ethanol, through the addition of photogenerated electrons (e$^-$) and hydrogen-ions (H$^+$). Further interaction of ethanol with another formyl-radical may have generated propionaldehyde, which may have produced propanol through the
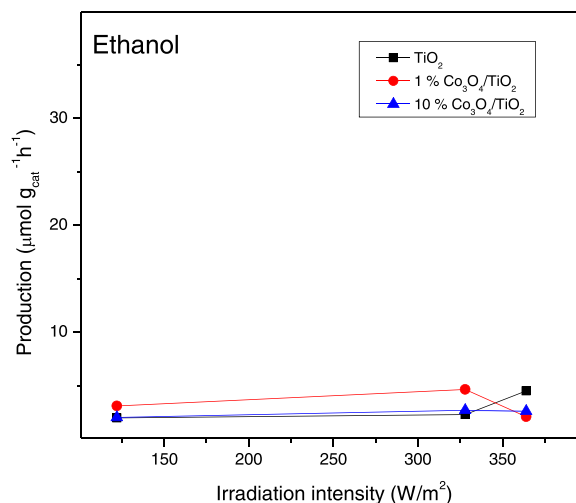

Fig. 18. Ethanol production on TiO$_2$-based photocatalysts as a function of visible irradiation intensity.

addition of photogenerated electrons (e⁻) and hydrogen ions (H⁺). The interaction of acetaldehyde with a methyl-radical may have generated isopropanol.
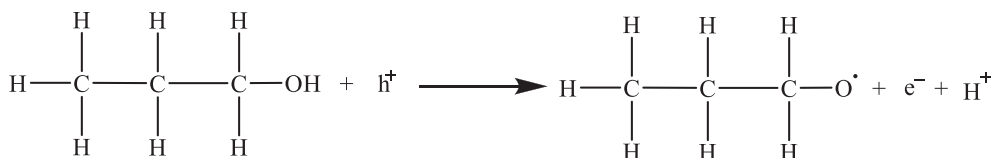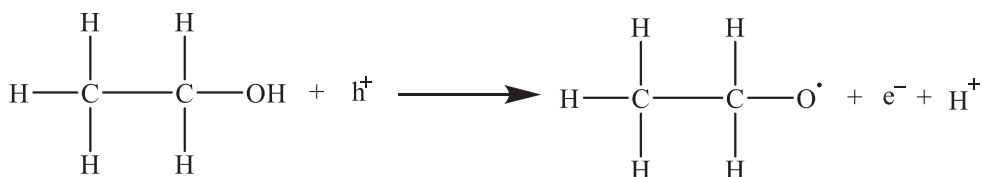
3.5.4. Effect of visible irradiation intensity on alcohols generation

The results of the quantitative analysis of the gas samples obtained during photocatalytic CO_2 reduction irradiated with 60-watt light bulb (328 W/m²) are presented in Table 8. In Tables S1 and S2, we reported the results of the quantitative analysis of the gas samples obtained during photocatalyzed CO_2 reduction irradiated with 14-watt led spotlight (122 W/m²) and with 100-watt light bulb (364 W/m²) respectively. In these tables, it can be seen that for the different visible light irradiation intensities, the main products detected were ethanol, propanol and isopropanol. However, the amounts of each generated alcohol, depended on the visible irradiation intensity.

Fig. 17 shows isopropanol evolution during the process as a function of visible irradiation intensity. In the figure, it can be observed, that for the three photocatalysts, isopropanol production increases with irradiation intensity reaching a maximum value at 328 W/m². However, higher irradiation intensity (364 W/m²) resulted in a decrease in isopropanol concentration. The result is in agreement with previous investigations that demonstrated that too high irradiation intensity increases the identical concentrations in electrons-holes, increasing the recombination rate, resulting in a decrease of the generated products [68].

Figs. 18 and 19 show respectively, ethanol and propanol production, generated during the photocatalytic process as a function of visible irradiation intensity. The figures show, slight variations of ethanol and propanol production with irradiation intensity. These alcohols productions should have shown a similar behavior to that of isopropanol, manifesting a maximum production at a given value of irradiation intensity. However, this was not the case.

These results may not imply that the ethanol and propanol generations are independent of irradiation intensity or only depend slightly on it. This observation can be explained, considering that produced ethanol and propanol molecules, dissolved in the reacting aqueous medium, being in close proximity to the photocatalyst surface, might have reacted as electron donors, through photocatalytic oxidation, according to the following reactions:

.

Fig. 19. Propanol production on TiO_2-based photocatalysts as a function of visible irradiation intensity.

generation rates might have been similar to their photocatalytic oxidation rates. As these photocatalytic reactions are directly dependent on the irradiation intensity, their rates might have been similar at the three visible irradiation intensities studied, resulting in the observed slight variations on ethanol and propanol concentrations with irradiation intensity.

Since isopropanol is also an alcohol, its photocatalytic oxidation might have also taken place, thus its production evolution with irradiation intensity should have been similar to that of ethanol and propanol. This fact cannot be ruled out. However, isopropanol being a secondary alcohol, may present a lower adsorption rate at the photocatalyst surface, than that of ethanol and propanol (primary alcohols), resulting in a lower photocatalytic oxidation probability. On the other hand, as can be seen in Table S4 (Supplementary Information), the isopropanol oxidation potential is higher than ethanol and propanol oxidation potentials. This fact indicates that isopropanol photocatalytic oxidation probability is lower than that of ethanol and propanol.

The results of the quantitative analysis for hydrogen peroxide (H_2O_2) yield are presented in Table 7, for photocatalytic CO_2 reduction during

.

The generated e⁻ and H⁺ through alcohols oxidation, might have further produced other alcohols molecules through the direct photocatalytic CO_2 reduction. The ethanol and propanol photocatalytic
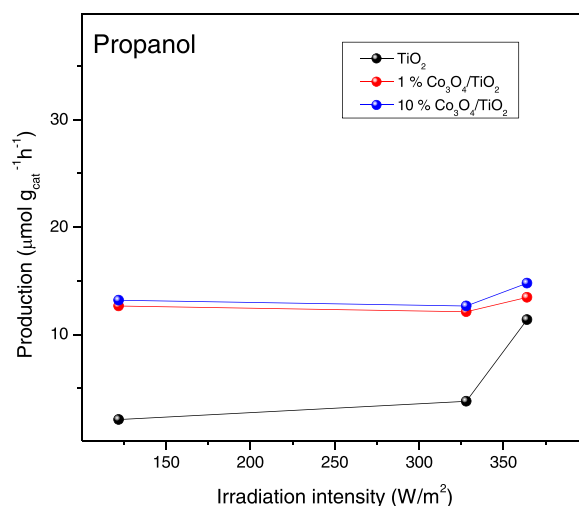
irradiation with UV light using TiO_2, $1\%Co_3O_4/TiO_2$ and $10\%Co_3O_4/TiO_2$ as photocatalysts. In Fig. S6, it can be observed a linear correspondence between H_2O_2 and ethanol yields. Hydrogen peroxide, being an oxidation product, may have enhanced the photocatalytic CO_2

reduction, resulting in an increase in ethanol production. However, the propanol and isopropanol yield values observed in Table 7, do not indicate any relation at all with hydrogen peroxide yield. The result suggests that the reductant effect of H_2O_2 for alcohols production takes place mainly at the first stages of the photocatalytic process, increasing mainly ethanol production, which is produced during the first stages of the process. As the photocatalytic process further proceeded, photocatalytic hydrogen peroxide oxidation could have been hindered by the completive adsorption, not only of the reactants and the reaction intermediaries, but also by the adsorption of the produced ethanol and propanol molecules at the photocatalysts surface-active sites. Moreover, as can be seen in Table S4 (Supplementary Information), the hydrogen peroxide oxidation potential is much higher than that of ethanol, propanol, isopropanol and water, therefore, photocatalytic H_2O_2 oxidation, would be less probable than that of the other molecules present during the photocatalytic CO_2 reduction.

4. Conclusions

The results presented in this investigation, demonstrated the use of Co_3O_4/TiO_2 photocatalyst for efficient alcohols production during CO_2 photoreduction with H_2O, using UV or visible light as radiation sources. Co/TiO_2 calcined at 900 °C resulted in Co_3O_4 nanoparticles formation on the TiO_2 surface. The high activity of the photocatalysts for alcohols production is attributed to the presence of Ti^{3+}, Co^{2+} and Co^{3+} which, on one hand decrease the TiO_2 band-gap energy and the photogenerated electron-hole recombination process. On the other hand, Ti^{3+}, Co^{2+} and Co^{3+} improve adsorption of CO_2 and of generated CO on the photocatalyst surface, increasing the formyl-radical formation rate, which is the essential step for the production of ethanol and propanol during CO_2 photoreduction with H_2O.

The design experiments results revealed that the cobalt concentration has a significant effect on alcohol total production at optimal metal concentration in 1%Co_3O_4/TiO_2. The high metal concentration in 10% Co_3O_4/TiO_2 is detrimental to CO_2 photoreduction, due to the higher metal ion species concentration, which increases the electron-hole recombination probability. The irradiation intensity parameter showed that the photocatalysts studied have a photoexcitation limit, i.e. the increase of intensity irradiance does not increase the total alcohol production from CO_2 photoreduction with H_2O.

CRediT authorship contribution statement

Daniel Montalvo: Investigation and Methodology. **Grisel Corro:** Concepualization, Investigation, Supervision, Writing – original draft, Writing – review and editing. **Fortino Bañuelos:** Formal analysis, Investigation. **Octavio Olivares-Xometl:** Data curation and editing. **Paulina Arellanes:** Formal analysis, Editing. **Umapada Pal:** Formal analysis, Editing.

Declaration of Competing Interest

The authors declare that they have no known competing financial interests or personal relationships that could have appeared to influence the work reported in this paper.

Data availability

No data was used for the research described in the article.

Acknowledgements

Appendix A. Supporting information

Supplementary data associated with this article can be found in the online version at doi:10.1016/j.apcatb.2023.122652.

References

[1] C. Mardones, N. Baeza, Economic and environmental effects of a CO_2 tax in Latin American countries, Energy Policy 114 (2018) 262–273, https://doi.org/10.1016/j.enpol.2017.12.001.

[2] S.H. Mohr, J. Wang, G. Ellem, J. Ward, D. Giurco, Projection of world fossil fuels by country, Fuel 141 (2015) 120–135, https://doi.org/10.1016/j.fuel.2014.10.030.

[3] A. Valadkhani, R. Smyth, J. Nguyen, Effects of primary energy consumption on CO_2 emissions under optimal thresholds: Evidence from sixty countries over the last half century, Energy Econ. 80 (2019) 680–690, https://doi.org/10.1016/j.eneco.2019.02.010.

[4] M. McGee, Global CO_2 emissions, CO_2, Earth (2022). ⟨https://www.co2.earth/global-co2-emissions⟩. accessed October 6, 2022.

[5] J.I. Santos, A.E. Cesarin, C.A.R. Sales, M.B.B. Triano, Increase Atmosphere CO_2 Conc. Its Eff. Cult. /Weed Interact. 11 (2017) 8.

[6] N. Shehzad, M. Tahir, K. Johari, T. Murugesan, M. Hussain, A critical review on TiO2 based photocatalytic CO_2 reduction system: strategies to improve efficiency, J. CO_2 Util. 26 (2018) 98–122, https://doi.org/10.1016/j.jcou.2018.04.026.

[7] K. Li, X. An, K.H. Park, M. Khraisheh, J. Tang, A critical review of CO_2 photoconversion: catalysts and reactors, Catal. Today 224 (2014) 3–12, https://doi.org/10.1016/j.cattod.2013.12.006.

[8] P.N. Paulino, V.M.M. Salim, N.S. Resende, Zn-Cu promoted TiO2 photocatalyst for CO_2 reduction with H2O under UV light, Appl. Catal. B Environ. 185 (2016) 362–370, https://doi.org/10.1016/j.apcatb.2015.12.037.

[9] F. Almomani, R. Bhosale, M. Khraisheh, A. Kumar, M. Tawalbeh, Photocatalytic conversion of CO_2 and H2O to useful fuels by nanostructured composite catalysis, Appl. Surf. Sci. 483 (2019) 363–372, https://doi.org/10.1016/j.apsusc.2019.03.304.

[10] R. Chong, Y. Fan, Y. Du, L. Liu, Z. Chang, D. Li, Hydroxyapatite decorated TiO2 as efficient photocatalyst for selective reduction of CO_2 with H2O into CH4, Int. J. Hydrog. Energy 43 (2018) 22329–22339, https://doi.org/10.1016/j.ijhydene.2018.10.045.

[11] G. Qin, Y. Zhang, X. Ke, X. Tong, Z. Sun, M. Liang, S. Xue, Photocatalytic reduction of carbon dioxide to formic acid, formaldehyde, and methanol using dye-sensitized TiO2 film, Appl. Catal. B Environ. 129 (2013) 599–605, https://doi.org/10.1016/j.apcatb.2012.10.012.

[12] L. Wang, S. Cao, K. Guo, Z. Wu, Z. Ma, L. Piao, Simultaneous hydrogen and peroxide production by photocatalytic water splitting, Chin. J. Catal. 40 (2019) 470–475, https://doi.org/10.1016/S1872-2067(19)63274-2.

[13] F. Zhang, Y.H. Li, M.Y. Qi, Y.M.A. Yamada, M. Anpo, Z.R. Tang, Y.J. Xu, Photothermal catalytic CO_2 reduction over nanomaterials, Chem. Catal. 1 (2021) 272–297, https://doi.org/10.1016/j.checat.2021.01.003.

[14] L. Yuan, M.Y. Qi, Z.R. Tang, Y.J. Xu, Coupling strategy for CO_2 valorization integrated with organic synthesis by heterogeneous photocatalysts, Angew. Chem. Int. Ed. 60 (2021) 21150–21172, https://doi.org/10.1002/anie.202101667.

[15] H. Abdullah, Md.M.R. Khan, H.R. Ong, Z. Yaakob, Modified TiO 2 photocatalyst for CO 2 photocatalytic reduction: an overview, J. CO_2 Util. 22 (2017) 15–32, https://doi.org/10.1016/j.jcou.2017.08.004.

[16] Y. Zhao, Y. Wei, X. Wu, H. Zheng, Z. Zhao, J. Liu, J. Li, Graphene-wrapped Pt/TiO2 photocatalysts with enhanced photogenerated charges separation and reactant adsorption for high selective photoreduction of CO_2 to CH4, Appl. Catal. B Environ. 226 (2018) 360–372, https://doi.org/10.1016/j.apcatb.2017.12.071.

[17] A. Khalilzadeh, A. Shariati, Photoreduction of CO_2 over heterogeneous modified TiO2 nanoparticles under visible light irradiation: synthesis, process and kinetic study, Sol. Energy 164 (2018) 251–261, https://doi.org/10.1016/j.solener.2018.02.063.

[18] L. Zhang, M. Jaroniec, Toward designing semiconductor-semiconductor heterojunctions for photocatalytic applications, Appl. Surf. Sci. 430 (2018) 2–17, https://doi.org/10.1016/j.apsusc.2017.07.192.

[19] W. Hou, W.H. Hung, P. Pavaskar, A. Goeppert, M. Aykol, S.B. Cronin, Photocatalytic Conversion of CO 2 to Hydrocarbon Fuels via Plasmon-Enhanced Absorption and Metallic Interband Transitions, ACS Catal. 1 (2011) 929–936, https://doi.org/10.1021/cs2001434.

[20] L. Spadaro, F. Arena, P. Negro, A. Palella, Sunfuels from CO_2 exhaust emissions: Insights into the role of photoreactor configuration by the study in laboratory and industrial environment, J. CO_2 Util. 26 (2018) 445–453, https://doi.org/10.1016/j.jcou.2018.05.010.

[21] M. Tahir, Photocatalytic carbon dioxide reduction to fuels in continuous flow monolith photoreactor using montmorillonite dispersed Fe/TiO2 nanocatalyst, J. Clean. Prod. 170 (2018) 242–250, https://doi.org/10.1016/j.jclepro.2017.09.118.

[22] Y. Wei, X. Wu, Y. Zhao, L. Wang, Z. Zhao, X. Huang, J. Liu, J. Li, Efficient photocatalysts of TiO2 nanocrystals-supported PtRu alloy nanoparticles for CO_2 reduction with H2O: Synergistic effect of Pt-Ru, Appl. Catal. B Environ. 236 (2018) 445–457, https://doi.org/10.1016/j.apcatb.2018.05.043.

[23] B. Yu, Y. Zhou, P. Li, W. Tu, P. Li, L. Tang, J. Ye, Z. Zou, Photocatalytic reduction of CO 2 over Ag/TiO 2 nanocomposites prepared with a simple and rapid silver mirror method, Nanoscale 8 (2016) 11870–11874, https://doi.org/10.1039/C6NR02547A.

[24] B. Tahir, M. Tahir, N.A.S. Amin, Photocatalytic CO2 conversion over Au/TiO2 nanostructures for dynamic production of clean fuels in a monolith photoreactor, Clean. Technol. Environ. Policy 18 (2016) 2147–2160, https://doi.org/10.1007/s10098-016-1181-4.

[25] F. Zhang, Y.H. Li, M.Y. Qi, Z.R. Tang, Y.J. Xu, Boosting the activity and stability of Ag-CuO2/ZnO nanorods for photocatalytic CO2 reduction, Appl. Catal. B 268 (2020), 118380, https://doi.org/10.1016/j.apcatb.2019.118380.

[26] K.Q. Lu, Y.H. Li, F. Zhang, M.Y. Qi, X. Chen, Z.R. Tang, Y.M.A. Yamada, M. Anpo, M. Conte, Y.J. Xu, Rationally designed transition metal hydroxide nanosheet arrays on graphene for artificial CO2 reduction, Nat. Commun. 11 (2020) 5181, https://doi.org/10.1038/s41467-020-18944-1.

[27] Y.H. Chen, M.Y. Qi, Y.H. Li, Z.R. Tang, T. Wang, J. Gong, Y.J. Xu, Activating two-dimensional Ti3C2Tx-MXene with single-atom cobalt for efficient CO2 photoreduction, Cell. Rep. Phys. Sci. 2 (2021), 100371, https://doi.org/10.1016/j.xcrp.2021.100371.

[28] Merck, Sigma-Aldrich, (n.d.). ⟨https://www.sigmaaldrich.com/MX/es/search/7440%E2%80%9348–4?focus=products&page=1&perpage=30&sort=relevance&term=7440%E2%80%9348–4&type=product⟩ (accessed July 3, 2022).

[29] W. Wang, T. Li, S. Komarneni, X. Lu, B. Liu, Recent advances in Co-based co-catalysts for efficient photocatalytic hydrogen generation, J. Colloid Interface Sci. 608 (2022) 1553–1575, https://doi.org/10.1016/j.jcis.2021.10.051.

[30] M. Tahir, N.S. Amin, Photocatalytic CO2 reduction with H2O vapors using montmorillonite/TiO2 supported microchannel monolith photoreactor, Chem. Eng. J. 230 (2013) 314–327, https://doi.org/10.1016/j.cej.2013.06.055.

[31] Y. Li, C. Wang, M. Song, D. Li, X. Zhang, Y. Liu, TiO2-x/CoOx photocatalyst sparkles in photothermocatalytic reduction of CO2 with H2O steam, Appl. Catal. B Environ. 243 (2019) 760–770, https://doi.org/10.1016/j.apcatb.2018.11.022.

[32] H. Feng, J. Zhang, X. Wang, T.H. Lee, Analysis of auto-ignition characteristics of low-alcohol/iso-octane blends using combined chemical kinetics mechanisms, Fuel 234 (2018) 836–849, https://doi.org/10.1016/j.fuel.2018.07.008.

[33] M.A. Ghadikolaei, P.K. Wong, C.S. Cheung, Z. Ning, K.-F. Yung, J. Zhao, N.K. Gali, A.V. Berenjestanaki, Impact of lower and higher alcohols on the physicochemical properties of particulate matter from diesel engines: a review, Renew. Sustain. Energy Rev. 143 (2021), 110970, https://doi.org/10.1016/j.rser.2021.110970.

[34] Md.M. Khan, R.P. Sharma, A.K. Kadian, S.M.M. Hasnain, An assessment of alcohol inclusion in various combinations of biodiesel-diesel on the performance and exhaust emission of modern-day compression ignition engines – A review, Mater. Sci. Energy Technol. 5 (2022) 81–98, https://doi.org/10.1016/j.mset.2021.12.004.

[35] A. Uyumaz, An experimental investigation into combustion and performance characteristics of an HCCI gasoline engine fueled with n-heptane, isopropanol and n-butanol fuel blends at different inlet air temperatures, Energy Convers. Manag. 98 (2015) 199–207, https://doi.org/10.1016/j.enconman.2015.03.043.

[36] L. Huang, B. Li, B. Su, Z. Xiong, C. Zhang, Y. Hou, Z. Ding, S. Wang, Fabrication of hierarchical Co 3 O 4 @CdIn 2 S 4 p–n heterojunction photocatalysts for improved CO 2 reduction with visible light, J. Mater. Chem. A 8 (2020) 7177–7183, https://doi.org/10.1039/D0TA01817A.

[37] J.R. Anderson, Structure of metallic catalysts, Academic Press, London; New York, 1975.

[38] G. Corro, J. Cruz-Mérida, D. Montalvo, U. Pal, Performance of Pt/Cr 2 O 3, Pt/ZrO 2, and, Pt/γ-Al 2 O 3 Catalysts in Total Oxidation of Methane: Effect of Metal–Support Interaction, Ind. Eng. Chem. Res. 60 (2021) 18841–18852, https://doi.org/10.1021/acs.iecr.1c02902.

[39] P. Makuła, M. Pacia, W. Macyk, How to correctly determine the band gap energy of modified semiconductor photocatalysts based on UV–Vis spectra, J. Phys. Chem. Lett. 9 (2018) 6814–6817, https://doi.org/10.1021/acs.jpclett.8b02892.

[40] S.E. Braslavsky, A.M. Braun, A.E. Cassano, A.V. Emeline, M.I. Litter, L. Palmisano, V.N. Parmon, N. Serpone, Glossary of terms used in photocatalysis and radiation catalysis (IUPAC Recommendations 2011, Pure Appl. Chem. 83 (2011) 931–1014, https://doi.org/10.1351/PAC-REC-09-09-36.

[41] W.-H. Lee, C.-H. Liao, M.-F. Tsai, C.-W. Huang, J.C.S. Wu, A novel twin reactor for CO2 photoreduction to mimic artificial photosynthesis, Appl. Catal. B Environ. 132–133 (2013) 445–451, https://doi.org/10.1016/j.apcatb.2012.12.024.

[42] V.R. Akshay, B. Arun, S. Dash, A.K. Patra, G. Mandal, G.R. Mutta, A. Chanda, M. Vasundhara, Defect mediated mechanism in undoped, Cu and Zn-doped TiO 2 nanocrystals for tailoring the band gap and magnetic properties, RSC Adv. 8 (2018) 41994–42008, https://doi.org/10.1039/C8RA07287F.

[43] C. Jin, B. Liu, Z. Lei, J. Sun, Structure and photoluminescence of the TiO2 films grown by atomic layer deposition using tetrakis-dimethylamino titanium and ozone, Nanoscale Res. Lett. 10 (2015) 95, https://doi.org/10.1186/s11671-015-0790-x.

[44] J. Liu, X. Ma, L. Yang, X. Liu, A. Han, H. Lv, C. Zhang, S. Xu, In situ green oxidation synthesis of Ti 3+ and N self-doped SrTiO x N y nanoparticles with enhanced photocatalytic activity under visible light, RSC Adv. 8 (2018) 7142–7151, https://doi.org/10.1039/C7RA13523H.

[45] L. Wang, T. Qi, J. Wang, S. Zhang, H. Xiao, Y. Ma, Uniform dispersion of cobalt nanoparticles over nonporous TiO2 with low activation energy for magnesium sulfate recovery in a novel magnesia-based desulfurization process, J. Hazard. Mater. 342 (2018) 579–588, https://doi.org/10.1016/j.jhazmat.2017.08.080.

[46] B. Bharti, S. Kumar, H.-N. Lee, R. Kumar, Formation of oxygen vacancies and Ti3+ state in TiO2 thin film and enhanced optical properties by air plasma treatment, Sci. Rep. 6 (2016) 32355, https://doi.org/10.1038/srep32355.

[47] L. Xu, Q. Jiang, Z. Xiao, X. Li, J. Huo, S. Wang, L. Dai, Plasma-Engraved Co 3 O 4 nanosheets with oxygen vacancies and high surface area for the oxygen evolution reaction, Angew. Chem. Int. Ed. 55 (2016) 5277–5281, https://doi.org/10.1002/anie.201600687.

[48] C. Alex, S.Ch Sarma, S.C. Peter, N.S. John, Competing Effect of Co 3+ reducibility and oxygen-deficient defects toward high oxygen evolution activity in Co 3 O 4 Systems in Alkaline Medium, ACS Appl. Energy Mater. 3 (2020) 5439–5447, https://doi.org/10.1021/acsaem.0c00297.

[49] J. Li, Z. Li, F. Ning, L. Zhou, R. Zhang, M. Shao, M. Wei, Ultrathin Mesoporous Co 3 O 4 Nanosheet Arrays for High-Performance Lithium-Ion Batteries, ACS Omega 3 (2018) 1675–1683, https://doi.org/10.1021/acsomega.7b01832.

[50] L. Zheng, H. Li, X. Xu, Catalytic decomposition of N 2 O over Mg-Co composite oxides hydrothermally prepared by using carbon sphere as template, J. Fuel Chem. Technol. 46 (2018) 569–577, https://doi.org/10.1016/S1872-5813(18)30024-0.

[51] B. Choudhury, A. Choudhury, Luminescence characteristics of cobalt doped TiO2 nanoparticles, J. Lumin. 132 (2012) 178–184, https://doi.org/10.1016/j.jlumin.2011.08.020.

[52] M. Hamadanian, A. Reisi-Vanani, A. Majedi, Sol-gel preparation and characterization of Co/TiO2 nanoparticles: Application to the degradation of methyl orange, J. Iran. Chem. Soc. 7 (2010) S52–S58, https://doi.org/10.1007/BF03246184.

[53] L. Collado, A. Reynal, F. Fresno, M. Barawi, C. Escudero, V. Perez-Dieste, J. M. Coronado, D.P. Serrano, J.R. Durrant, V.A. de la Peña O'Shea, Unravelling the effect of charge dynamics at the plasmonic metal/semiconductor interface for CO2 photoreduction, Nat. Commun. 9 (2018) 4986, https://doi.org/10.1038/s41467-018-07397-2.

[54] Q. Chen, F. Ji, T. Liu, P. Yan, W. Guan, X. Xu, Synergistic effect of bifunctional Co–TiO2 catalyst on degradation of Rhodamine B: Fenton-photo hybrid process, Chem. Eng. J. 229 (2013) 57–65, https://doi.org/10.1016/j.cej.2013.04.024.

[55] Y. Qu, W. Zhou, H. Fu, Porous cobalt titanate nanorod: a new candidate for visible light-driven photocatalytic water oxidation, ChemCatChem 6 (2014) 265–270, https://doi.org/10.1002/cctc.201300718.

[56] D.M. Tobaldi, L. Lajaunie, N. Rozman, A.P.F. Caetano, M.P. Seabra, A. Sever Škapin, R. Arenal, J.A. Labrincha, Impact of the absolute rutile fraction on TiO2 visible-light absorption and visible-light-promoted photocatalytic activity, J. Photochem. Photobiol. Chem. 382 (2019), 111940, https://doi.org/10.1016/j.jphotochem.2019.111940.

[57] H. Song, G. Zhou, C. Wang, X. Jiang, C. Wu, T. Li, Synthesis and photocatalytic activity of nanocrystalline TiO2 co-doped with nitrogen and cobalt(II, Res. Chem. Intermed. 39 (2013) 747–758, https://doi.org/10.1007/s11164-012-0594-x.

[58] H. G, S. S, G. P, M.K. Shrivash, D. Kumar, Synthesis of chromium doped cobalt oxide (Cr:Co3O4) nanoparticles by co-precipitation method and enhanced photocatalytic properties in the visible region, J. Mater. Sci. Eng. 07 (2018), https://doi.org/10.4172/2169-0022.1000419.

[59] L. Xiuhua, F. Yibei, Studies on the Structures and Optical Properties of Tio2 Doped with Transition Metals, in: F. Marquis (Ed.), Proc. 8th Pac. Rim Int. Congr. Adv. Mater. Process, Springer International Publishing, Cham, 2013, pp. 295–305, https://doi.org/10.1007/978-3-319-48764-9_37.

[60] J.-J. Wang, Y.-H. Jing, T. Ouyang, Q. Zhang, C.-T. Chang, Photocatalytic reduction of CO2 to energy products using Cu–TiO2/ZSM-5 and Co–TiO2/ZSM-5 under low energy irradiation, Catal. Commun. 59 (2015) 69–72, https://doi.org/10.1016/j.catcom.2014.09.030.

[61] A. Olivo, E. Ghedini, M. Signoretto, M. Compagnoni, I. Rossetti, Liquid vs. Gas Phase CO2 photoreduction process: which is the effect of the reaction medium? Energies 10 (2017) 1394, https://doi.org/10.3390/en10091394.

[62] Scope and prospect of transition metal-based cocatalysts for visible light-driven photocatalytic hydrogen evolution with graphitic carbon nitride, in: A. Kumar Singh, C. Das, A. Indra (Eds.), Coord. Chem. Rev., 465, 2022, 214516, https://doi.org/10.1016/j.ccr.2022.214516.

[63] P. Usubharatana, D. McMartin, A. Veawab, P. Tontiwachwuthikul, Photocatalytic process for CO 2 emission reduction from industrial flue gas streams, Ind. Eng. Chem. Res. 45 (2006) 2558–2568, https://doi.org/10.1021/ie0505763.

[64] O. Ola, M.M. Maroto-Valer, Transition metal oxide based TiO2 nanoparticles for visible light induced CO2 photoreduction, Appl. Catal. Gen. 502 (2015) 114–121, https://doi.org/10.1016/j.apcata.2015.06.007.

[65] R. Dholam, N. Patel, A. Miotello, Efficient H2 production by water-splitting using indium–tin-oxide/V-doped TiO2 multilayer thin film photocatalyst, Int. J. Hydrog. Energy 36 (2011) 6519–6528, https://doi.org/10.1016/j.ijhydene.2011.03.028.

[66] N. Serpone, D. Lawless, J. Disdier, J.-M. Herrmann, Spectroscopic, photoconductivity, and photocatalytic studies of TiO2 colloids: naked and with the lattice doped with Cr3+, Fe3+, and V5+ Cations, Langmuir 10 (1994) 643–652, https://doi.org/10.1021/la00015a010.

[67] A. Olivo, W.A. Thompson, E.R.B. Bay, E. Ghedini, F. Menegazzo, M. Maroto-Valer, M. Signoretto, Investigation of process parameters assessment via design of experiments for CO2 photoreduction in two photoreactors, J. CO2 Util. 36 (2020) 25–32, https://doi.org/10.1016/j.jcou.2019.10.009.

[68] J.-M. Herrmann, Photocatalysis fundamentals revisited to avoid several misconceptions, Appl. Catal. B Environ. 99 (2010) 461–468, https://doi.org/10.1016/j.apcatb.2010.05.012.

[69] N.N. Greenwood, A. Earnshaw. Chemistry of the Elements, 2nd ed.,, Butterworth-Heinemann,, 1997, p. 1118. ISBN 978-0-08-037941-8.

[70] G.M. Kale, S.S. Pandit, K.T. Jacob, Thermodynamics of Cobalt (II, III) Oxide (Co3O4): evidence of phase transition, Trans. Jpn. Inst. Met. 29 (1988) 125–132, https://doi.org/10.2320/matertrans1960.29.125.

[71] Y. Vieira, K. da Boit Martinello, T.H. Ribeiro, J.P. Silveira, J.S. Salla, L.F.O. Silva, E. L. Foletto, G.L. Dotto, Photo-assisted degradation of organic pollutant by CuFeS2

powder in RGB-LED reactors: A comprehensive study of band gap values and the relation between wavelength and electron-hole recombination, Adv. Powder Technol. 33 (2022), 103368, https://doi.org/10.1016/j.apt.2021.11.020.

[72] J. Qiu, G. Zeng, M. Ge, S. Arab, M. Mecklenburg, B. Hou, C. Shen, A.V. Benderskii, S.B. Cronin, Correlation of Ti3+ states with photocatalytic enhancement in TiO2-passivated p-GaAs, J. Catal. 337 (2016) 133–137, https://doi.org/10.1016/j.jcat.2016.02.002.

[73] M.T. Greiner, M.G. Helander, W.-M. Tang, Z.-B. Wang, J. Qiu, Z.-H. Lu, Universal energy-level alignment of molecules on metal oxides, Nat. Mater. 11 (2012) 76–81, https://doi.org/10.1038/nmat3159.

[74] Y. Ji, Y. Luo, Theoretical study on the mechanism of photoreduction of CO_2 to CH_4 on the anatase TiO_2(101) surface, ACS Catal. 6 (2016) 2018–2025. ⟨https://doi.org/10.1021/acscatal.5b02694⟩.